J. theor. Biol. (2002) **216,** 301–326
doi:10.1006/yjtbi.2540, available online at http://www.idealibrary.com on IDEAL®

Exploring the Formation of Alzheimer's Disease Senile Plaques *in Silico*

LEAH EDELSTEIN-KESHET*† AND ATHAN SPIROS

†*Department of Mathematics, University of British Columbia, Vancouver BC, Canada, V6 T 1Z2*

(*Received on* 28 *August* 2001, *Accepted in revised form on* 15 *January* 2002)

An experimental simulation environment suitable for exploring the neuroinflammatory hypothesis of Alzheimer's disease (AD) has been developed. Using scientific literature, we have calculated parameters and rates and constructed an interactive model system. The simulation can be manipulated to explore competing hypotheses about AD pathology, i.e. can be used as an experimental "*in silico*" system. In this paper, we outline the assumptions and aspects of the model, and illustrate qualitative and quantitative findings. The interactions of amyloid beta deposits, glial cell dynamics, inflammation and secreted cytokines, and the stress, recovery, and death of neuronal tissue are investigated. The model leads to qualitative insights about relative roles of the cells and chemicals in the disease pathology.

An *In Silico* Experimental System

Biological experiments have traditionally been carried out *in vivo* or *in vitro.* Recent interest has grown in the new setting of "*in silico*" experiments, i.e. those carried out in the setting of detailed computer simulation models where hypotheses can be tested. *In silico* systems could ideally provide an initial platform for drug target triage, rapidly identifying the pathways most likely or rejecting those least likely to lead to positive outcomes: see Eddershaw *et al.* (2000), Norris *et al.* (2000), Gray & Keck (1999). An *in silico* system is not meant to replace traditional biological experiments, but, rather, to complement them. As a theoretical framework, such systems can help to identify key relationships that might be hard to ascertain from the complexity of the biological system.

Recent examples of *in silico* systems include ECELL by Tomita *et al.* (1999), Virtual Cell (Schaff *et al.*, 1997; Fink *et al.*, 2000), and simulations of biochemical pathways by Palsson (2000); these are systems that explore events at the level of single cells or small groups of cells, internal biochemical pathways, or distribution of substances inside cellular compartments. Other recent applications include experimental tests of the effect of permuting genomes for fitness of a bacteriophage T7 (Endy *et al.*, 2000). The business models of several companies (e.g. Entelos, Physiome) are based on such systems, though their work is proprietary and not available for open discussion in the wider scientific community.

In this paper, we describe a preliminary online *in silico* simulation for neuroinflammation and pathology associated with Alzheimer's disease (AD). We outline the background of the pathology, the way that we modeled and simulated the various known and hypothesized interactions, the tests carried out to study the system, and what we learned from these. As we show, the ability to accurately portray details of this complex disease is challenging, and perhaps beyond immediate reach. However, some qualitative and quantitative results are obtainable even

*Author to whom correspondence should be addressed.
E-mail: keshet@math.ubc.ca

0022-5193/02/$35.00/0

in cases where not all details are known, or where parts of the system are not explicitly included.

Alzheimer's Disease

Alzheimer's disease is associated with progressive death of neurons in the central nervous system (CNS). Specific pathology includes senile plaques (Fig. 1), amyloid deposits [Fig. 1(a)], and abnormal cytoskeletal structures (neurofibrillary tangles). Certain genotypes cause increased propensity, but the details of the genetic vs. environmental causes are uncertain. As the disease develops over a period of years, perceptible changes in cognition and memory occur only at advanced stages, when a significant fraction of neurons have died.

The statistics of Alzheimer's disease (AD) are frightening: in the year 1998, nearly 23 000 deaths from AD were recorded in the U.S.A. alone, amounting to 2.6 deaths per 100 000 individuals, and making AD the ninth leading cause of U.S.A. death (National Vital Statistics Reports, Vol. 48, No. 11). According to the Alzheimer's Association, it is estimated that more than 22 million individuals worldwide will be affected by the year 2025; this rate of incidence will include 10% of all individuals over age 65, and almost 50% of those over age 85. The time span from onset of symptoms to death varies from 8 to 20 years. Some of the key aspects of the disease are described below.

Biological Background

AMYLOID-BETA

Amyloid-beta (A-beta) plays a dominant role in AD. This is a small peptide, roughly 3–4 kDa in size (40–42 amino acids). Amyloid-beta is cut by enzymes from a segment of a large (695 amino acids) trans-membrane protein called amyloid precursor protein (APP). The mean level of soluble A-beta is much higher in Alzheimer's disease than in normal individuals, and correlates with severity of the disease (McLean *et al.*, 1999). In familial AD, production of amyloid-beta protein is elevated up to six-fold over normal levels (Cai *et al.*, 1993).

Soluble amyloid-beta (in the form of monomers) diffuses freely through neuronal tissue; at elevated levels, it produces pathological aggregates, fibers, and persistent deposits that cannot be readily cleared. According to Come *et al.* (1993), formation of an initial "seed" is a rate-determining step for aggregation. Sites of amyloid deposition in AD form diffuse plaques, and are believed to develop into mature senile plaques that are associated with stress and death of neurons (Fig. 1; see also Itakagi *et al.*, 1989). Physiological levels of metal ions [e.g. Cu(II) and Zn (II)] accelerate amyloid aggregation (Bush *et al.*, 1994) causing nanomolar levels of A-beta to aggregate in 15 min [Moir *et al.* (1999); see Bush *et al.* (1994) for rate constants]. Other factors that influence A-beta dynamics include apolipoprotein (the APOE4 allele is a known risk factor for AD), pH, α1 anti-chymotrypsin (α1 ACT) and other amyloid-associated proteins (Akiyama *et al.*, 2000).

There are numerous studies on morphology (Christie *et al.*, 2001), size distribution (Hyman *et al.*, 1995), density (Itakagi *et al.*, 1989), and correlation of senile plaques to AD severity. Benes *et al.* (1989) proposed the idea that a senile plaque results from diffusion of amyloid outwards from some source. A theoretical treatment of plaque development was proposed by Urbanc *et al.* (1997, 1999), Cruz *et al.* (1997) as a process of aggregation and disaggregation with no specific underlying mechanism. In this paper, we look in greater detail at the underlying events causing deposition, uptake, removal, and degradation of amyloid, as well as a number of hypotheses for chief determinants of neuronal stress, going beyond what was proposed in the above reference. In particular, we investigate some of the feedback mechanisms that perpetuate the problem once it has been initiated.

GLIAL CELLS

Glial cells (including microglia and astrocytes) are non-neuronal cells with various functions in the healthy brain [Fig. 1(b) and (c)]. The roles of microglia and astrocytes in the pathology of AD is described below.

Microglia

Microglia are non-neuronal cells that play an important part in the immune system of the

brain (Streit and Kincaid-Colton, 1995). In their resting state in the brain, microglia are highly ramified cells. Under conditions of injury or stress, they undergo successive stages of activation, and reactivity: changing morphology and becoming compact, motile, chemotactic, and phagocytic. A primary role of phagocytic microglia is removal of foreign substances, debris and dead material. In mature plaques, reactive microglia are generally found clustered at the plaque core [Fig. 1(c)]. The distribution of microglia in the AD brain, and their relationship to amyloid deposits are described by Itakagi *et al.* (1989).

Microglia participate in an inflammatory response, signal other glial and neuronal cells (via cytokines), secrete a variety of immune-related substances (e.g. Complement), generate free radicals, as well as act as a clean-up crew in charge of clearing amyloid deposits. According to Giulian *et al.* (1994), reactive microglial products mediate activation of astrocytes as well as neuronal injury. Substances that lead to the activation of microglia (e.g. the bacterial endotoxin lipopolysaccharide, LPS) are correlated with neuronal toxicity. Evidence suggests that with normal human aging, microglia become increasingly reactive in the brain (Sheng *et al.*, 1997). Further, differences in the density of microglia may explain why some parts of the brain are more prone to inflammation or found to develop a higher density of senile plaques (Kim *et al.*, 2000).

Reactive microglia are attracted to and move towards amyloid (and other soluble substances) by chemotaxis (Davis *et al.*, 1992; Nolte *et al.*, 1996, 1997). However, fibrous amyloid immobilizes the microglia and also results in the production of reactive oxygen species (Shaffer *et al.* 1995; El Khoury *et al.*, 1996, Fig. 3). Adhesion is affected by the presence of soluble amyloid (e.g. Fig. 1(a) and (b) in El Khoury *et al.*, 1996). Microglia are known to take up beta-amyloid in the soluble form. Fibrous amyloid is removed by microglia by phagocytosis, but tends to be relatively resistant to degradation.

Astrocytes

Astrocytes participate in the cycle of inflammation. They become activated by microglial cytokines, notably IL-1B (Hu & Van Eldik, 1999), and secrete a variety of chemical factors, including the cytokines (Griffin *et al.*, 1996). Like microglia, astrocytes can migrate in the central nervous system, though details of this motion in the adult brain are not well known. In mature senile plaques in the AD brain, astrocytes are found mostly gathered around the periphery of a plaque [Fig. 1(b)]. Here they form a "shell" or "scar tissue" encasing the plaque (Griffin *et al.*, 1996). There is evidence suggesting that astrocytes produce barriers that seal off affected areas. Astrocytes may also affect the way that microglia uptake and clear amyloid from plaque-associated deposits (Shaffer *et al.*, 1995; Akiyama *et al.*, 1999). According to Shaffer *et al.* (1995) astrocyte secretions reduce the ability of microglia to process amyloid.

CYTOKINES

A variety of potent chemical signaling molecules, collectively known as cytokines, mediate inflammation in the brain. Among these are the interleukins (IL-1 beta, IL-6), and tumor necrosis factor (TNF-α). IL-1beta (IL-1B), secreted predominately by reactive microglia, occurs at elevated levels early in the development of a plaque. IL-1B activates the production and processing of APP in the tissue, leading to a possible increase in amyloid-beta production (Mrak *et al.*, 1995, 2000; Donnelly *et al.*, 1990; Buxbaum *et al.*, 1992; Forloni *et al.*, 1992). In this way, IL-1B contributes to the formation of new sources of amyloid in a kind of positive feedback that can accelerate formation of plaques and destruction of neurons (see schematic diagram, Fig. 2). IL-1B activates astrocytes, promoting their secretion of IL-6, TNF, and S100-beta (Mrak *et al.*, 1995, 2000; Sheng *et al.*, 1996). IL-1B has also been shown to be directly toxic to neurons (*in vitro*) at high concentrations (Mrak *et al.*, 2000). Evidence thus points to IL-1B as a major factor driving the disease (Sheng *et al.*, 1996).

The cytokine IL-6 occurs at high levels during normal nervous system development, but is virtually undetectable in healthy adult brain. In Alzheimer's disease, IL-6 is produced at high levels by activated astrocytes as part of the

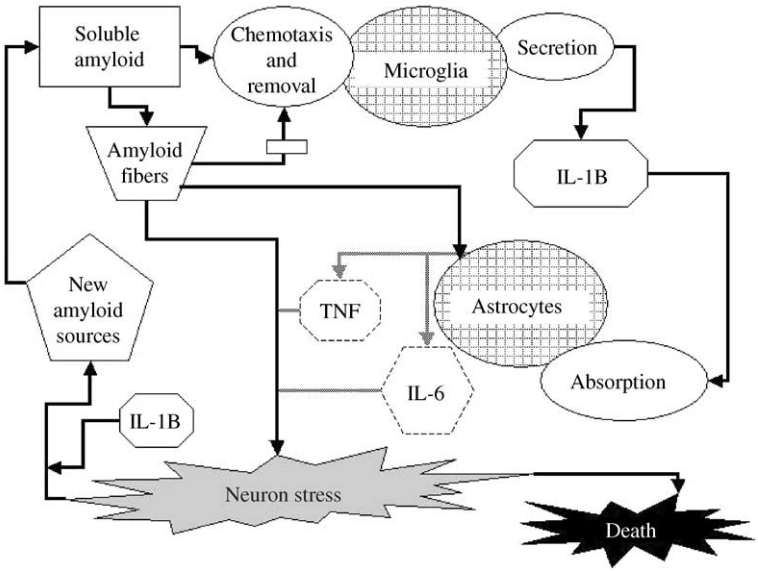

FIG. 2. Schematic diagram showing some of the interactions considered in the simulation. Soluble amyloid causes microglial chemotaxis, and activates IL-1B secretion. Astrocytes activated by IL-1B secrete cytokines TNF and IL-6. Neurons uptake IL-1B and produce new amyloid sources. A variety of assumptions were explored about what causes stress and death of neurons.

inflammatory cycle. It is believed that IL-6 is injurious and destructive. (Mutations that reduce the expression of IL-6 are also associated with delayed AD progression.) Ma & Zhu (2000) showed that low levels of IL-6 kill neurons and suggested that cell death results from nitric oxide accumulation.

Controversy surrounds the role of TNF. Known to be toxic in the body to specific tumor cells, its role in the brain has been identified as destructive by some (Gelbard *et al.*, 1993) and/or protective by others (Cheng *et al.*, 1994; Tarkowski *et al.*, 1999). Conflicting ideas may stem from differences in experimental conditions, or may be related to the fact that there are different cell-surface receptors for TNF (p55 and p75) that probably play distinct roles. The p55 receptor is linked to the intracellular apoptosis signal, whereas the p75 may be protective (Akiyama *et al.*, 2000).

FIG. 1. Light microscope images of senile plaques and arrangement of glial cells in human AD brain. (a) Staining for amyloid-beta-42, showing the characteristic morphology and distribution of amyloid at plaques. (b) Localization of microglia in the center (CR3-43 stain) and surrounding ring of astrocytes (star-like shapes, GFAP stain) at a plaque site. (c) Congregation of microglia (dark shapes, CR3-43 stain) and nuclei of other cells (neutral red stain) at a plaque. Small tick marks represent 0.01 mm (i.e. 10 μm) in each frame. Images kindly supplied by Claudia Schwab and used with permission of the McGeer group, Kinsmen Laboratory, University of British Columbia.

FIG. 4. The secretion of the cytokine IL-1B (not here shown) by microglia is assumed to promote processing of APP and lead to new sources of beta amyloid in the tissue. This results in the formation of new plaque sites at the periphery of the initial plaque, or possibly much heavier deposition of fiber in the central plaque. The stochastic nature of the simulation means that the number of new sources, and their locations are somewhat random, leading to quite variable results. The diameter of the plaque in (c) is about 120 μm. Results shown for runs with fast neuronal dynamics lasting 800 min in parts (a)–(d) and slower neuronal dynamics and fiber deposition (over a period of 10 days) in parts (e)–(h).

FIG. 7. A variety of shapes and sizes of plaques obtained with astrocytes included in the interactions. Parts (a)–(d) were produced with fast neuron and fiber deposition dynamics ($r = 0.1$, $e_F = 1.51$) Parts (e) and (f) were produced with slower neuronal health dynamics ($r = 0.01$, $e_F = 0.1499$). The overall results are quite similar qualitatively. Length of bar: 100 μm.

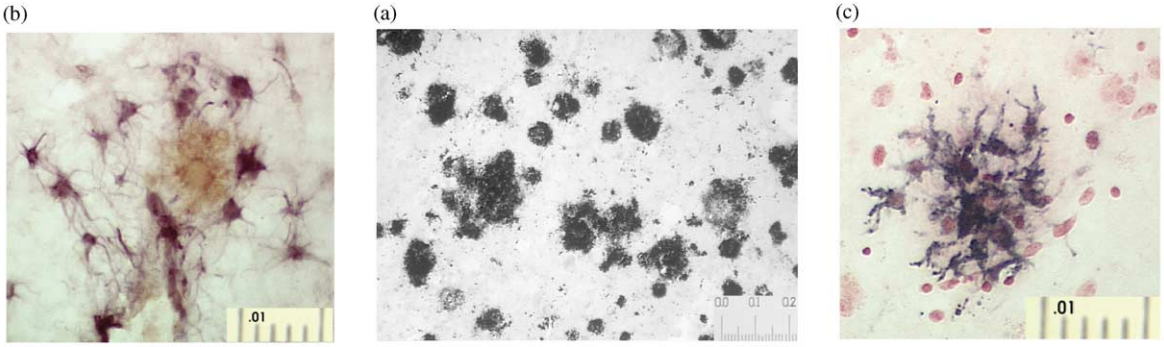

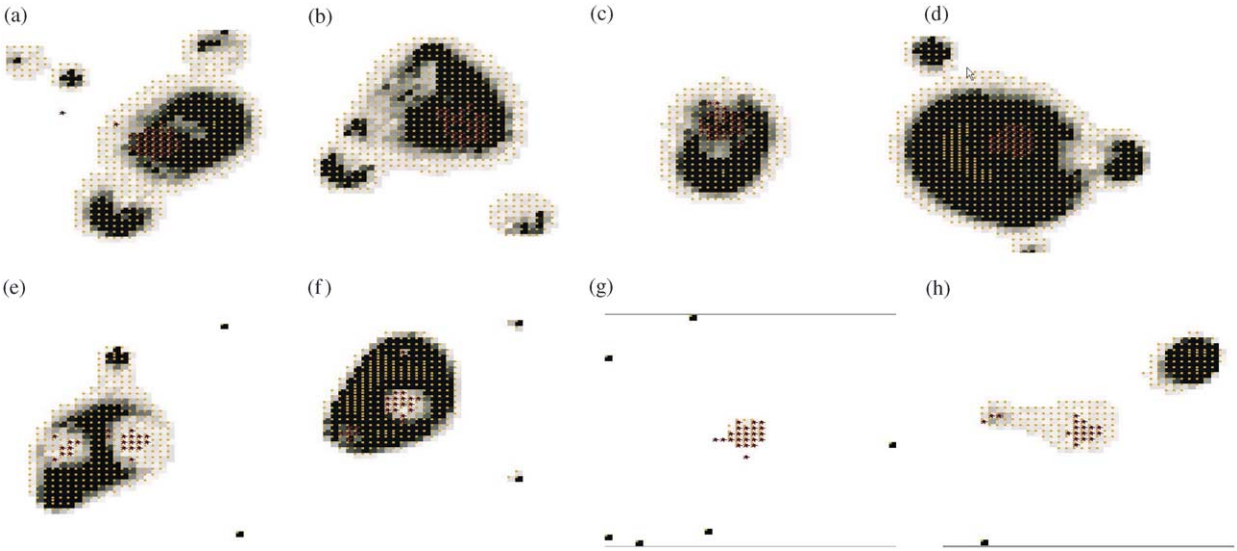

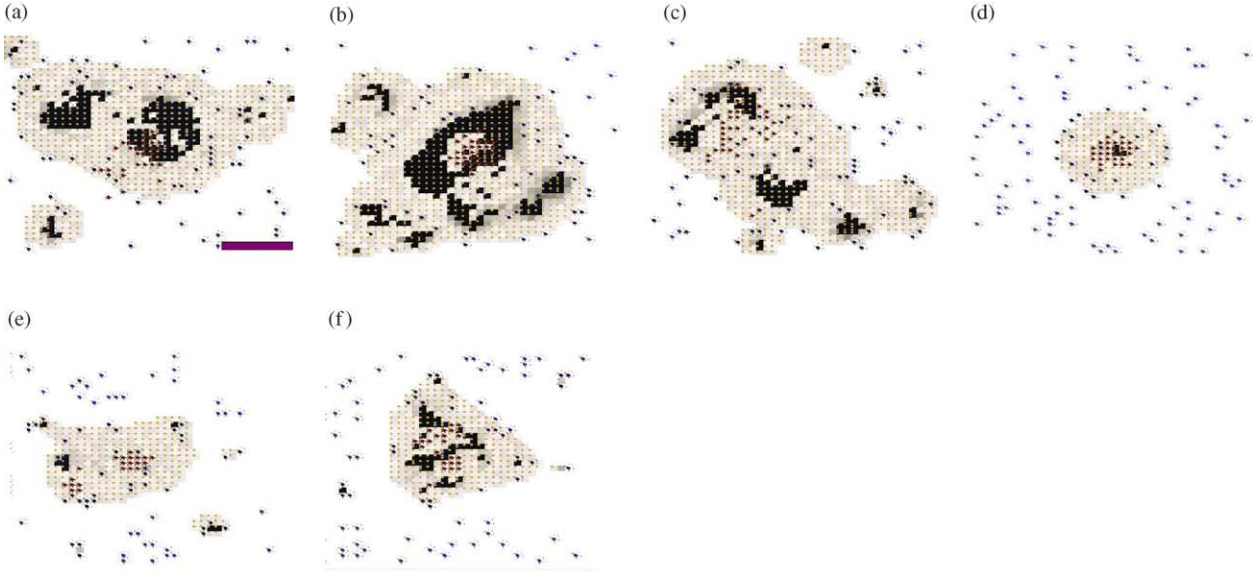

doi:10.1006 jtbi.2002.2540

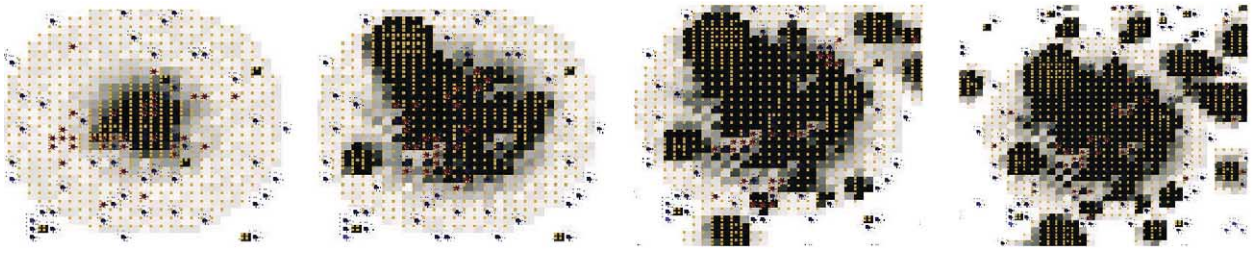

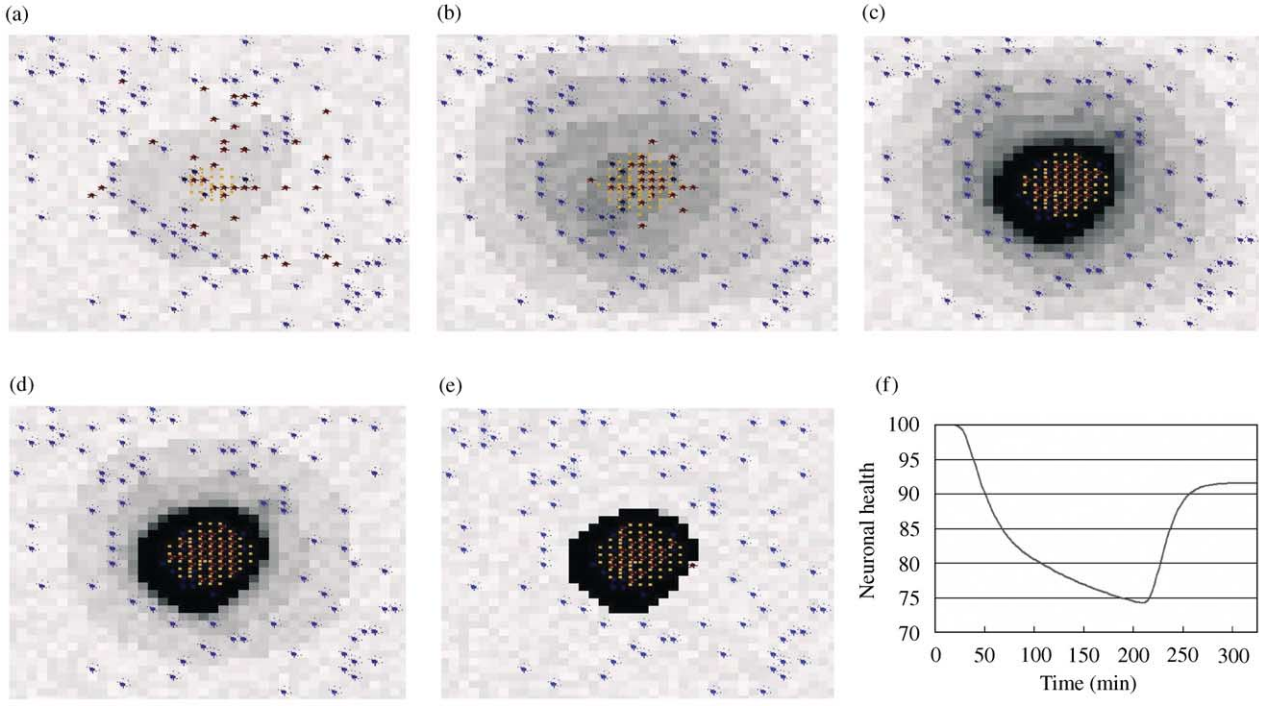

doi:10.1006 jtbi.2002.2540

INFLAMMATION AND NEUROTOXICITY IN AD

One of the currently held hypotheses is that an inflammatory cycle drives AD pathology (Fig. 2; see also McGeer & McGeer, 1995, 1998a, b, 1999). Feedback and feedforward effects of cytokines on glial cells and neurons amplify initial stimuli into rampant runaway responses. These responses consist of cytokine cycles (Griffin *et al.*, 1996, 1998; Mrak *et al.*, 1995), and production of a variety of factors such as complement, chemokines, inflammatory and acute phase proteins, α-1 anti-chymotrypsin (reviewed in Akiyama *et al.*, 2000). Head trauma, or infection that results in inflammation are known as risk factors for AD (Griffin *et al.*, 1996; Brugg *et al.*, 1995).

Death of neurons depends on a balance between injurious and protective effects. The toxicity of a factor need not necessarily be a direct killing: in many cases the actual effect may be excitotoxic (over-stimulating the neuron, or induction of excess glutamate that overwhelms the cell), induced production of reactive oxygen species that damage the cell or its components, or inhibition of protective mechanisms. There is agreement in much of the literature that amyloid deposits are deleterious. (Amyloid toxicity caused by induced calcium influx and reactive oxygen species is discussed by Ekinci *et al.* (2000) and Michaelis *et al.* (1998).) Further, toxicity of amyloid-beta to neuronal cells in culture has been found to depend on its form: some studies suggest that fibrillar amyloid is more toxic than soluble amyloid (Moir *et al.*, 1999 and references therein) other investigators (e.g. McLean *et al.*, 1999) find that mean level of soluble, but *not* fibrous amyloid beta, correlates highly with markers of disease severity.

The effects of cytokines are more controversial. Direct or indirect toxicity of cytokines at elevated levels has been reported but little is known about the mechanisms (Bocci, 1998). Cheng *et al.* (1994) argued that TNF-α is neuroprotective (by leading to an increase in calcium-binding proteins, e.g. in rat neurons). Carlson *et al.* (1999) argued that TNF-α, IL-1α, IL-1B, and IL-6 are neuroprotective to an excitotoxic influx of calcium mediated through neuronal (NMDA) glutamate-gated ion channels. Gelbard *et al.* (1993) found that TNF-α is neurotoxic through activation of AMPA receptors. Chao *et al.* (1995) found that IL-1beta and TNF-α, were injurious in combination, and attributed this to induction of nitric oxide (NO) production by astrocytes. Cytokine treatments can also have synergistic effects (Jeohn *et al.*, 1998). According to Stoll *et al.* (2000), some cytokines such as TNF-α and IL-1beta may have double roles: in the presence of inducible NO synthase (iNOS) they are neurotoxic while in the absence of iNOS, they enhance neuroprotection and plasticity.

The time-scale on which significant neuronal death occurs in AD brains is many years (*in vivo*), resulting in slow decline in mental function in affected elderly patients. However, this cognitive decline is noticeable only when the disease is in an advanced form, making it hard to deduce the time-scale on which injury, repair, and neuronal death takes place locally, i.e. close to foci at which pathological events are initiated. The development of plaques is hard enough to follow non-invasively (see Christie *et al.*, 2001). The level of health or stress of neurons on a local level is even harder to assess *in vivo*. The slow overall development of AD symptoms may stem

FIG. 10. The evolution of a growing plaque under the effect of astrocyte blocking is shown here (for another parameter set) at times $t = 50$, 300, 750, and 1200 min. Astrocytes significantly affect the morphology of the plaque, leading to an irregular central dead region surrounded by smaller "sprouts" in places where the toxic influence of amyloid has leaked through breaks in the sealed-off region.

FIG. 11. (a)–(e): A typical time sequence ($t = 40$, 80, 200, 230, 270 min from left to right, top to bottom) showing changes in neuron health due to a diffusible toxic product of activated astrocytes. The amyloid source causing microglia to secrete IL-1B was gone by $t = 130$ (due to neuronal death). This eventually stopped astrocytic secretion, but stress and further death continued until about $t = 210$, due to time for gradual removal and decay of the inflammatory substances. Once the chemical levels had fallen, a fairly rapid recovery occurred in those regions that had not died, leaving a small core of dead neurons in the center. Here amyloid fiber has no effect on neuronal health directly. (f) A plot of the neuronal health for this time sequence.

from one of several factors: (1) it may result from accumulation of very rare initiation events, (2) it may be due to efficient localization and containment of the injurious effects so that they rarely spread beyond small affected regions, or (3) it may stem from inherently slow dynamics of neuronal death at all size scales. In the first two cases, we may still study significant local events at a time-scale that is much shorter than the time-scale of the disease as a whole. The third possibility is less likely, given the known sensitivity of neuronal cells to toxic or excitotoxic effects, but if this were the case, then a simulation of local events on the time-scale of minutes, hours, or days would be an inappropriate tool for studying the disease. On the other hand, in vitro experiments, using tissue cultures of undifferentiated human neuroblastoma cells, reveal significant mortality in response to various secretions produced by stimulated microglia within times on the order of 24 h (Klegeris *et al.*, 1999). The process of apoptosis (programmed cell death) known to occur in damaged cells takes place on a time-scale of 1–24 h. This means, at the very least, that experimental investigations of neurotoxicity on this time-scale are not wholly unreasonable. Similar arguments bridging the time-scale of individual and local events to overall disease progression appear in Clarke *et al.* (2000, 2001).

The Simulation

The purpose of the simulation is to dissect and understand how a limited number of parts, believed to be implicated in AD, fit together (Fig. 2). In this study, we aim to incorporate more detail than previous models (e.g. Urbanc *et al.*, 1997, 1999), while maintaining a level of simplicity that allows dissection and analysis. The controversial state of the discipline makes it difficult to identify detailed disease progression scenarios that are uniformly believed by the community. However, part of the strength of modeling and simulation is that they can test a wide variety of hypothetical mechanisms, at various levels of detail. Hypotheses or subsystems that produce unrealistic predictions are informative: they can indicate which parts of the pathology cannot be accounted for when certain key components or interactions are missing. Clearly, we do not claim to reproduce the Alzheimer's disease pathology in its full complexity, a daunting goal that remains beyond reach currently.

Brain structures and AD plaques (Cruz *et al.*, 1997) are three dimensional. In our online Java-based simulation, restrictions on computational speed, memory, and visualization techniques limited the initial investigation reported here to a 2D setting, representing a thin square slice of neural tissue ($400 \times 400\,\mu m^2$, with assumed depth $10\,\mu m$.) A time-scale of minutes is used to follow cell motion and molecular diffusion. Diffusion of peptides is rapid relative to movement and interactions of cells. Thus, we use a short time step to compute chemical diffusion, and a longer time step for calculating cell movement and changes in the states of cells (e.g. from inactive to active). The simulation accurately depicts diffusion and cell motion. When prolonged runs are made, typical time-scale of neuronal degeneration (hours, days, or weeks) can be followed. In this study we have made many preliminary short-term runs to gain some appreciation of the events on a short time-scale, as well as some longer runs to understand the interplay between neuron health dynamics and these short-term events.

The idea of the simulation is to investigate the cascade of events that follow downstream of an initial inflammation-provoking stimulus, injury, or defect. Accordingly, we assume that one "infected site" provokes a tissue response. To represent this, a single source of soluble amyloid-beta ("the stimulus") is placed in the center of a region of healthy neuronal tissue in the initial state of the system. A population of microglia, astrocytes, and some foci of amyloid fiber seeds are placed randomly in the region at frequencies that are adjustable parameters. The simulation begins with the diffusion of soluble amyloid from its source, and attraction of microglia by chemotaxis to soluble amyloid.

MOLECULAR DIFFUSION

The diffusion coefficient of a soluble peptide can be estimated from its molecular weight (see Appendix.) We used a standard approximation

to estimate diffusion coefficients of all appropriate chemicals. Diffusion in the brain is slowed by tissue structure and inhomogeneities. We corrected for the average tortuosity of brain tissue (described in Sykova, 1997; Nicholson & Sykova, 1998), and for local changes in tissue properties that evolve over time (see effects of astrocytes, described below). Typical effective diffusion coefficients that we use are given in Tables 1–3 in Appendix.

Chemicals are treated using deterministic, continuous kinetics, i.e. we numerically solve a discretized version of the 2D diffusion equation for each substance, expressed in the flux-based form:

$$\frac{\partial}{\partial t}c(x,y,t) = -\nabla \cdot \mathbf{J}(x,y,t) + \sigma(x,y,t),$$
$$\mathbf{J}(x,y,t) = -D(x,y,t)\nabla c.$$

Here $c(x,y,t)$ is the concentration of the given chemical at a point (x,y) and time, t, $D(x,y,t)$ its diffusion coefficient, and $\mathbf{J}(x,y,t)$ the diffusive flux of the substance. (Initially, D is constant. Later, should astrocytes be present, it may change over time in a spatially localized way.) Sources of chemicals (at secreting cells) are represented by the term σ.

We found that the above formulation was useful in meeting the challenge of correctly simulating diffusion in cases where the material properties of the region were not homogeneous. When astrocytes encounter fibrous deposits, we model their tendency to seal-off these regions as a local reduction in rates of diffusion of chemicals, as described below. This means that diffusion coefficients vary temporally and spatially. A numerical method based on the above flux formulation of the diffusion equation (in 2D) was chosen to minimize artifacts such as spurious amplification of concentrations that can arise in such discrete computations. (see Appendix for details).

CELL TYPES

Cell types included in the simulation are microglia, astrocytes, and neurons. Initially, the region contains a uniform tissue of healthy neurons. Glial cells of both types are distributed randomly over the domain. (The numbers of microglia and astrocytes are adjustable parameters.) Motion and state transitions of cells are incorporated in a Monte-Carlo fashion. (An explanation and further details are given in Appendix.) Motion of glial cells includes a chemotaxis component with some superimposed random motion, both governed by adjustable parameters. Cells are represented by moving points or graphic images, but to avoid excessive computational expense, each moving particle ("agent") in the simulation represents cumulative effects of some number of actual cells. The number of glial cells that can occupy a given grid site is limited, and the presence of one type of cell may exclude other types from entering the same grid space. Cells secrete and absorb chemicals at their current grid space.

MOTION OF MICROGLIA

Microglia move in a direction biased by the gradient of soluble amyloid with probability set by an adjustable chemotactic sensitivity parameter. Microglia are excluded from places already occupied by astrocytes or too many other microglia.

The motion of microglia next to fibrous and soluble amyloid is based on data and parameter values extracted from El Khoury *et al.* (1996): their Fig. 1(a) describes how microglia adhere to fibrillar amyloid at various concentrations; their Fig. 1(b) shows how soluble amyloid blocks this adherence. Based on those data, a Michaelis–Menten-type relationship (i.e. a simple saturating curve) was used to fit the probability that a microglial cell would stick to fiber at a given concentration, and a decreasing exponential dependence on the soluble amyloid concentration was assumed (see Appendix.)

AMYLOID PRODUCTION, AGGREGATION, AND REMOVAL

The simulation starts with a single site of soluble amyloid at the center of the domain that diffuses outwards over the region. This source persists until turned off manually, or until neurons at the given site have died.

When the level of soluble amyloid exceeds some critical value associated with fibrillization, fibrous deposits form in one of several ways:

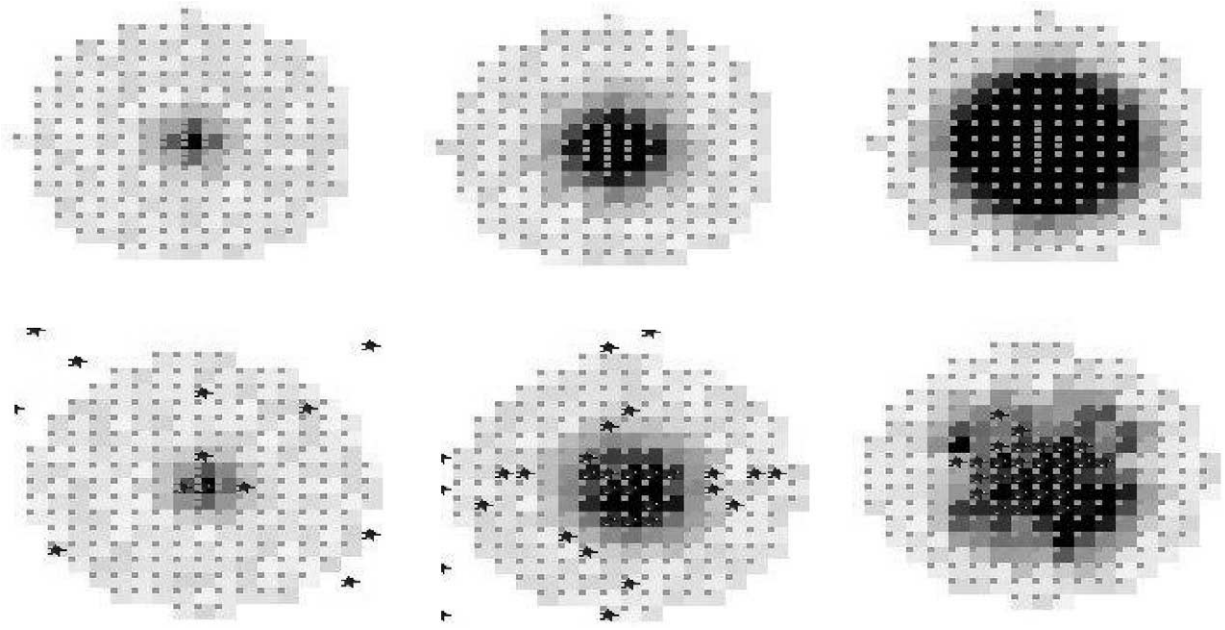

FIG. 3. Top row: Formation of a plaque and death of neurons in the absence of glial cells, when fibrous amyloid is the only injurious influence. The simulation was run with no astrocytes or microglia, and health of neurons was determined solely by the local fibrous amyloid. Shown above is a time sequence (left to right) of three stages in plaque development, at early, intermediate, and advanced stage. Density of fibrous deposit is represented by small dots and neuronal health by shading from white (healthy) to black (dead). Note radial symmetry due to simple diffusion. Bottom row: Effect of microglial removal of amyloid on plaque morphology. Note that microglia (small star-like shapes) are seen approaching the plaque (via chemotaxis to soluble amyloid, not shown). At a later stage, they have congregated at the plaque center, where they adhere to fibers. As a result of removal of soluble and fibrous amyloid, the microglia lead to irregular plaque morphology. Size scale: In this and all other figures, the distance between the small single dots (representing low fiber deposits) is 10 μm. Similar results obtained for a ten-fold scaling in the time-scale of neuronal health dynamics.

where there are pre-existing fibers, growth by elongation takes place (up to some maximal density) at a rate that depends on the presence of both fibrous and soluble forms by simple mass-action kinetics. Fibers in one site can also elongate into adjoining sites. These processes are all computed by Monte-Carlo methods. A low level of *de novo* fiber nucleation occurs at empty sites away from deposits (Come *et al.*, 1993). It is assumed that fiber deposition rate increases dramatically when the level of soluble amyloid is far above its critical threshold for nucleation.

Amyloid removal is carried out by microglia. Tissue culture experiments have resulted in quantitative estimates of the rate of uptake (Shaffer *et al.*, 1995; El Khoury *et al.*, 1996; Ard *et al.*, 1996). We have assumed Michaelis–Menten kinetic forms and parameters for removal of soluble and fibrous amyloid, based on that experimental data. Microglia cannot uptake amyloid in excess of some maximal capacity, and they ingest amyloid fibers at some low basal rate. We assume that microglia neutralize and/or degrade the amyloid that they have absorbed.

Our simulation includes the induction of new sources of amyloid by IL-1B: this means that when neurons have absorbed IL-1B secreted by microglia, there is some probability that new sites of amyloid production will be formed in the tissue, leading to new foci of inflammation. This feature is meant to represent the increased processing of APP known to occur in the presence of elevated IL-1B (see Mrak *et al.*, 1995, 2000; Donnelly *et al.*, 1990; Buxbaum *et al.*, 1992; Forloni *et al.*, 1992).

CYTOKINES: RATES OF SECRETION

In the simulation, IL-1beta is secreted by microglia, and IL-6 and TNF are secreted by astrocytes. Microglia begin to secrete IL-1B

when their internal concentration of soluble amyloid exceeds some level needed for triggering secretion. Astrocytes secrete IL-6 and TNF once they have been activated by exposure to IL-1B. Details of the activation are given below. The rates of secretion of cytokines are based on data in Lee *et al.* (1993), Fiala *et al.* (1998), Van Wagoner *et al.* (1999). Typical rates of secretion, in units appropriate to the simulation are given in Table A2 and described in Appendix.

CYTOKINE UPTAKE

We use Michaelis–Menten kinetics to describe cytokine-receptor binding and resulting uptake of cytokines by cells. This standard assumption is based on a fixed number of receptors, saturation of receptors as ligand concentration increases, and uptake of ligand bound to the receptor. To estimate appropriate values for the Michaelean parameters we found information for typical equilibrium dissociation constants, K_D for IL-1B, TNF, and IL6 cytokines and their cell-surface receptors. In a few rare cases, we also found cited values for forward- and reverse-binding constants, as well as half-life of the receptors. One difficulty is that values we found come from a variety of species, cell types and conditions and may be very different for in vivo human cortical neurons. This problem is a major challenge facing *in silico* models, in general, and deserves wider recognition and discussion. Another problem is that receptors tend to be up- or down-regulated as a result of exposure to ligand: this was not taken into account at this stage of our investigation.

Values of receptor rate constants on which the simulation is based are shown in Table A3 in Appendix A. Information about the number of receptors per cell was also obtained from the literature. Since we are not modeling individual neurons, we had to calculate the approximate "receptor concentration per unit volume" (units of μM) in case of cytokine uptake by neurons.

ASTROCYTES

We wanted to represent the ability of astrocytes to "gather" at the periphery of plaques as seen in Fig. 1(b) and as described by Itakagi *et al.* (1989). To do so, we assigned four states to astrocytes: *inactive, receptive, motile, blocking*. Transitions between the first three states are assumed to depend on exposure to IL-1B (see, e.g. Hu & Van Eldik, 1999) with uptake assumed in the form of Michaelis–Menten kinetics. These transitions are accompanied by an assumed change in the morphology: the diameter of the region in which an astrocyte senses any stimulus decreases from about 90 μm to about 60 μm as they become motile. They then move a short distance by a biased random walk (max speed 0.1 μm/min: Kornyei *et al.*, 2000) in the direction of amyloid fiber. To avoid crowding, we assumed that astrocytes do not move into a site occupied by microglia, fiber, or too many other astrocytes.

We were also interested in depicting the fact that astrocytes form a kind of scar tissue around plaques, i.e. seal off the area and make it less permeable. To do this, we assigned a fourth state, called *blocking.* We assumed that transitions to the blocking state occur when an astrocyte senses and arrives at a fiber deposit. The cell becomes immobilized and starts to seal off the region. This is represented by a reduced rate of diffusion of substances in the vicinity. This leads to non-uniform spatial properties and has an interesting impact on the simulation outcomes that we discuss in a later section.

NEURONS

In the simulation, neurons are represented as a block of neuronal tissue, rather than a collection of individual neurons. Absorption of some chemicals (notably cytokines), secretion of others (such as amyloid-beta) and changes in health in response to conditions are incorporated into the simulation.

Absorption of IL-1B, IL-6 and TNF is modeled by receptor kinetics as described above. Production of new amyloid sources is promoted by IL-1B but can only occur in some maximal fraction of neurons (an adjustable parameter). New amyloid sources are currently active for the duration of the simulation or until neurons at the given site die. (We assumed that dead tissue is no longer capable of producing amyloid.)

In modeling the health of neurons, we had several requirements in mind: first, we do not intend, at this preliminary stage, to include

details of the intracellular events and signaling pathways that determine the fate of the neuron. Rather, we consider an aggregate parameter h, describing the local health of the neurons from 0 (dead) to 1 (100% healthy). (Currently, each site has a value of health, $0<h<1$, associated with it, and this value varies with time). Second, we wanted to satisfy several criteria: (1) An injurious effect should result in a decrease in health. Sub-lethal effects should merely depress the health without killing the neurons. (2) Below some minimal level of health, neurons should not recover. (3) Neurons above that minimal level should have innate capacity for recovery, so that removal of the affecting stimulus leads to eventual restoration of health. (4) Beyond some critical level of toxicity, the neurons should die. (5) Neurons that have been pre-stressed by some factors should be more susceptible to further injury or toxicity.

We found a simple deterministic rule that satisfies all above reasonable assumptions. The rule is described in a differential equation, that keeps track of changes in the health of the neuronal tissue at a given grid point as follows:

$$\frac{\mathrm{d}h}{\mathrm{d}t} = rh(1-h) - I.$$

Here, $r > 0$ is a recovery rate, and a time-dependent injury term, I (if positive) represents the level of toxicity at the given site. I depends on the environment at the given site, and its value changes as injurious chemicals accumulate. (It is worth noting that this differential equation is the well-known logistic equation with removal rate I. Similar equations are used to represent simple density-dependent population growth in the presence of a removal or harvesting term.) As described in the appendix and shown in Fig. A1, this equation has dynamical properties corresponding to requirements listed above, with several possible outcomes depending on relative recovery and injury rates. (i) In the absence of toxicity, every viable state evolves to full recovery. (ii) When toxicity is too high, recovery is too slow to compensate for the stressing influence: neurons in that site will all die. This can be prevented only if the injurious stimulus is removed before the neurons fall below their minimal health level. (iii) For sub-lethal toxicity, the outcome depends on the current state of the neurons: those whose health is too poor will die, whereas others will recover, but not to full health. While this simple differential equation cannot describe intricate aspects of health, stress and mortality, it suffices as an aggregate indicator for our purposes.

The rate of neuronal injury caused by a given factor (e.g. IL-1B, IL-6, TNF-α, etc.) is assumed to be proportional to the fraction, B_C, of cell-surface cytokine receptors bound on the given neuron. That fraction is taken to be a simple Michaelis–Menten function of the concentration of cytokine, C, at the given site:

$$B_C = \frac{C}{k_n + C}.$$

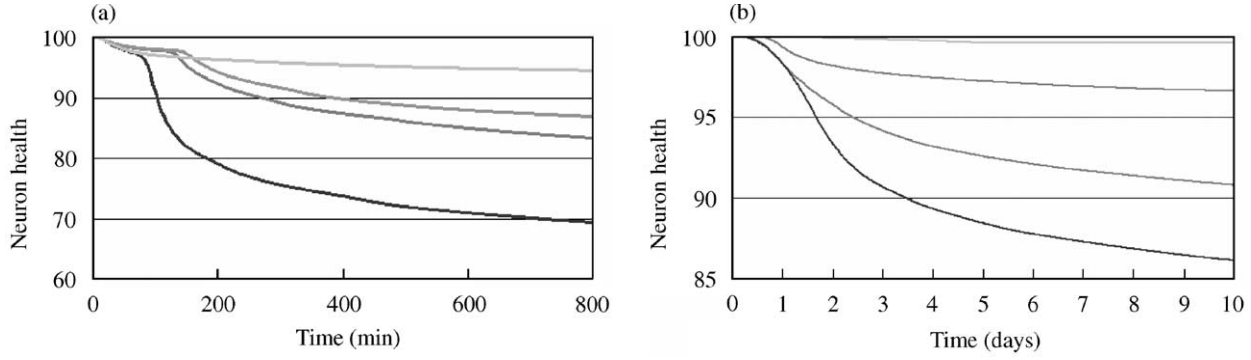

FIG. 5. Average neuron health over time, showing variability in the runs of Fig. 4. (a) For runs in parts (a)–(d) of Fig. 4. (b) For runs in parts (e)–(h) of Fig. 4.

Here k_n is the half-maximal binding concentration. This means that we are modeling the impact on health as an aggregate effect that stems from activation of cell-surface receptors, leaving out detail of what happens inside the cell beyond that point.

Soluble and fibrous amyloids are treated separately. We do not consider receptor binding, but rather direct cytotoxic effects, e.g. due to local redox reactions and oxidative stress (Huang *et al.* 1999a,b). Relative effects on health of soluble and fibrous amyloids are assumed to be simply proportional to the given amyloid concentration ($\boldsymbol{S}$, $\boldsymbol{F}$), scaled in some appropriate way (scale factors $\boldsymbol{S}_{max}$, $\boldsymbol{F}_{max}$).

The combined effect of various factors is calculated as follows. Each factor or substance is associated with a parameter, e_C, that describes its relative weight or influence. This parameter can be negative (signifying an injurious effect), zero (no effect), or positive (representing a neuroprotective influence). The values of these parameters can be changed interactively in our simulation to explore hypotheses about how competing destructive and neurotrophic influences interact, as described in the results section. The net injurious effect is computed by adding the contributions of all toxic and protective factors at the given site, leading to a cumulative expression as follows:

$$I = e_S \frac{S}{S_{\max}} + e_F \frac{F}{F_{\max}} + \sum_C e_C B_C.$$

In practice, many of the factors are assumed to be neutral in a given test case, as described in our results. For example, in one of the main cases we have explored (see next section), we assume that amyloid fiber is the toxic factor.

The average neuronal health in the region is determined by averaging the health of each of the $40 \times 40 = 1600$ sites in the region. This is plotted as a function of time for each run, as shown, for example in Fig. 5.

Experimental Exploration of the System

In this section, we summarize several results obtained by running the simulation under specific conditions. We explore the effects of certain small subsystems to dissect the influences of various cells and chemicals. Many of these cases were informative, particularly in their inability to match realistic plaques.

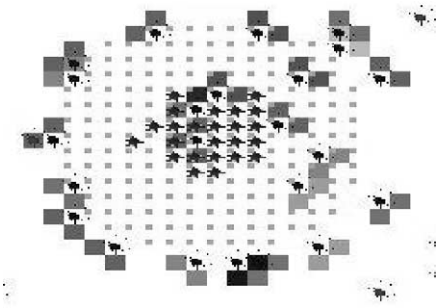

FIG. 6. Relative positions of microglia (star-shaped cells in center) and astrocytes (small fuzzy disks) next to a putative fiber deposit. Microglia have been attracted to an amyloid source at the center, and astrocytes have gathered at the edge of the fiber deposit. The effect of astrocytic blocking is shown by shaded areas. These shaded squares in this figure represent regions of reduced diffusion of chemicals.

Our simulation is best suited to time-scales associated with cell motion and diffusion. In some preliminary runs, we have assumed that neuronal health changes occur for a short time-scale of one or a few hours. Using longer simulations we verified that similar outcomes were obtained when the time-scale of the neuronal dynamics was much slower: many hours, days or even weeks. A complete list of default parameter values with meanings is given in our website and parameter sets corresponding to some of the runs are available and can be used to run the simulation.

SUBSYSTEMS

Amyloid and Neurons

Omitting glial cells, and considering only the production of amyloid and the effect of amyloid fiber on neurons, we obtained results shown in the time sequence (top row) of Fig. 3. For this experiment, we assumed that injury to neurons depended solely on amyloid fibers, and we set the recovery rate to zero ($r = 0$). This means that fiber deposits will always eventually kill neurons in their vicinity.

Initialization with a source of amyloid at the center of the domain created a local amyloid concentration above the threshold for nucleating

and maintaining fiber growth. The spread of amyloid, its conversion to fiber, and death of neurons followed a symmetrically expanding diffusion-limited disk. If fiber nucleation probability was low, the evolving plaque had a fractal appearance, as in diffusion-limited aggregation (DLA), whereas for higher rates of fiber deposition, the plaque was more radially symmetric. These observations match results of Cruz *et al.* (1997) who simulated growth of a 3D plaque as a process of aggregation of amyloid.

Size of the plaque was limited by the rate of amyloid conversion to fiber, and the toxicity of the fibers, since this, in turn, determined the length of time that the amyloid source was active. We ran two longer scale computations for periods equivalent to several days. Both cases had no neuronal recovery ($r = 0$), but in one, the effect of fiber on neuronal health was $e_F = 0.92$, and in the other it was $e_F = 0.04$, i.e. a factor of 20 less. The two results were very similar morphologically, with a 9.06% health decrease in the first case, and 10.08% decrease in the second over a period of 100 hr. Dead neurons were restricted to the site of the fiber deposits. Once the initial source was extinguished, amyloid concentration would fall below a critical level for fiber growth. At that point, the plaque stopped expanding, and very little further change occurred. [Compare with experimental results of Christie *et al.* (2001) who find little change in the majority of observed plaques over time-scales of 2 days to many months, but appearance of a few new plaques over the same time intervals.] If fiber deposition occurred only at very high amyloid levels (or else if fibers were highly toxic), the site of neuronal death would be restricted to the immediate proximity of the amyloid source.

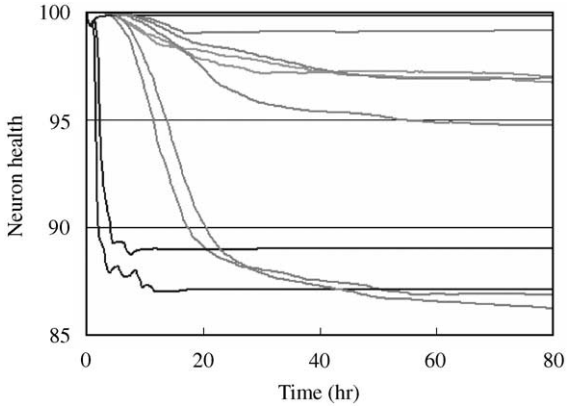

FIG. 8. Variability in outcomes and a comparison between fast and slow neuronal and fiber deposition dynamics for simulations similar to those of Fig. 7. The curves shown in black were obtained from runs with parameter set as in Fig. 7 (a)–(d) (fast neuron health dynamics) and the curves shown in gray were obtained from runs with the parameter sets used for Fig. 7 (e) and (f) (slow dynamics).

Amyloid, Neurons, and Microglia

We next investigated the effects of microglia on amyloid removal and on the evolution of the plaques described above. At first, we omitted cytokine signaling and focused only on the three most basic properties of microglia: (1) chemotaxis towards the amyloid source, (2) tendency to adhere to fibers, and (3) removal of both soluble and fibrous amyloid. [Here we are modeling a process that has been called "disaggregation" by Cruz *et al.* (1997), Urbanc *et al.* (1999) with a more detailed cell-based mechanism.] Results are shown in the bottom row of Fig. 3. We find that microglia congregate at the center of the plaque, where chemotaxis and adherence to fibers tend to dominate over random motion. Removal of amyloid by these glial cells leads to a more irregular plaque morphology, with a serrated edge and non-uniform internal

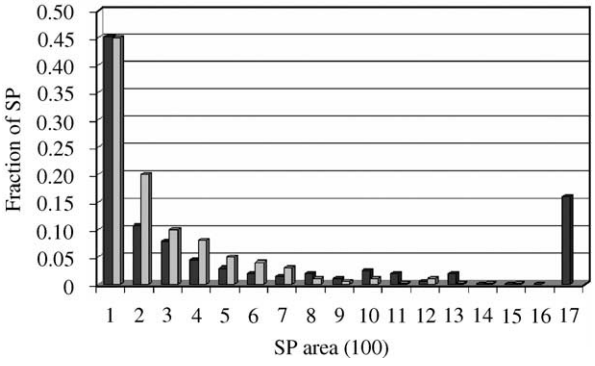

FIG. 9. Size distribution of the plaques obtained in runs with parameters as in Fig. 7 (dark bars) shown next to the size distribution obtained from an AD brain by Hyman *et al.* (1995) (light bars). The horizontal axis represents plaque areas in multiples of 100 μm^2. The last category represents all larger plaques that were obtained.

density. Results were similar for longer runs with more realistic, slow neuronal dynamics. However, if the source of amyloid persists for longer time due to a slower rate of death of affected neurons, the eventual size of the plaque tends to be somewhat larger in the simulation.

The Cytokine IL-1beta

We now included the secretion of the cytokine IL-1B by microglia, and its potential stimulation of new sources of amyloid. This leads to a positive feedback that has significant impact, leading to one of two distinctly new phenomena: (i) the formation of a number of new plaques in the region or (ii) massive growth and dominance of a very large plaque, with or without smaller offshoots. (The difference between these cases depends on the proximity of the amyloid sources to one another and the persistence time of those sources: sources forming close to one another, or lasting for a long time, tend to form a merged deposition of fiber, and large plaque size.) If the probability of new amyloid sources forming is too small, or the level of cytokine needed to produce such new sources is too high, the outcome is identical to previous experiments discussed above.

Typical outcomes of several runs are shown in Fig. 4. Parts (a)–(d) show plaques formed with accelerated neuronal dynamics. Parts (e)–(h) show outcomes with longer runs in which both fiber deposition and neuronal health changes are much slower, on a time-scale of many days. The corresponding temporal dynamics in these runs are shown in Fig. 5(a) (fast dynamics) and Fig. 5(b) (slow dynamics). The comparison reveals several notable facts: first, the overall qualitative comparison is robust—either one, several or very little plaque deposit will form in the region, with evidence for sprouts forming off a central site in cases (a), (b), (d), (e) and (h). [In case (h), the original site is not severely affected, but one of its offshoots grows.] Second, the temporal dynamics scale comparatively well, with a lag phase in each case, followed by a rapid decline that tapers off gradually. This type of declining health behavior has been referred to as the sigmoidal or increasing risk degeneration (Clarke *et al.*, 1999, 2000), and stems from the fact that over the time-scale of the simulation, toxicity is gradually building up in an initially healthy region. The significant difference between short and long time-scales is seen in the removal of amyloid by microglia. This affects fiber accumulation on the long time-scale to a greater extent, leading to more noticeable "holes" with resident microglia in plaques [4(e) and (f)].

If amyloid fiber deposition is much faster than neuronal degeneration, these types of results were not obtained. Then, to get similar behavior, it was necessary to assume that some factor aside from neuronal death limits the length of time that an amyloid source continues to produce amyloid. Manually turning off some of the new amyloid sources produced discrete plaques as in Fig. 4. Allowing amyloid sources to persist on the expanded time-scale of hours, could lead to massive accumulation of fiber throughout the domain and unrealistic behavior.

Similar experiments were carried out with many parameter settings: we varied the effect of amyloid fiber on neuronal health, the proportion of neurons that could give rise to new sources, the level of IL-1B that triggers those new sources, and the rate of recovery of neurons. We found that: (a) New sources can be formed even after the initial source has been removed, as accumulated IL-1B takes time to be depleted. (b) Microglia are then seen to chase one source after another, sometimes splitting up into separate groups. (c) For high amyloid production rate, fibrous deposits can become much heavier near the core of the plaque. This can trap and immobilize the microglia. (See assumptions we made about microglia motion.) (d) If the number of new sources is very high, there is a rapid acceleration in the decline of health after some time, since the uptake of amyloid by microglia saturates. (e) There is variability in runs with identical parameter values: some runs (e.g. lowest curves in Fig. 5) lead to significant decline of health over the given time period and large plaques. Other runs (e.g. highest curves) leave health nearly intact and no plaque formation at all. The causes and implications of this variability are discussed in a later section.

Toxicity of a Microglial Product

We asked what would be the outcome of toxicity of some product secreted by microglia in response to activation by amyloid. We ran several simulations in which fiber toxicity was removed, and replaced by toxicity of a microglial diffusible product. Results (not shown) can be described as follows: (a) toxicity begins when aggregated microglia are found in large numbers close to the attracting amyloid source that activates their secretion. The wave of stress and toxicity spreads outwards from this site. (b) Variations in the size of the product (i.e. in its rate of diffusion), in the secretion rate, the uptake rate, and/or impact on health determine how quickly the pathology develops, and the size of the necrotic region. (c) Individual runs are variable (see later discussion), and initiation of new amyloid sources strongly affects the severity of the outcome. (d) In contrast to previous results, motion of microglia (e.g. between an old source of amyloid and a new one) creates a "trail of death". Death of tissue correlates with sites of *reduced* fibrous deposits, since microglia remove amyloid fibers as they move across a developing plaque. (e) Once sources of amyloid are extinguished, gradual inactivation of microglia means that all slightly stressed regions that are not yet irretrievably damaged tend to recover. The end stage consists of a dead core of neurons, some fibrous deposits, in an otherwise healthy region.

It is premature to attempt here to identify which of the numerous factors secreted by microglia could play this specific neurotoxic role; complement, cytokines such as IL-1B, reactive oxygen species, proteases, etc. are possible candidates (Akiyama *et al*., 1999). These substances range in molecular size (and hence rates of diffusion in the brain) as well as rates of production by microglia, uptake by neurons, action on the cells, and impact on neuron health. In our simulation we currently include only one microglial product explicitly (modeled after properties of IL-1B), but each of the above parameters can be varied online interactively, to depict gross behavior of a range of sizes and actions of such molecules. We can in principle explore in detail a variety of possible chemical factors, but this was not our purpose here.

Astrocytes and their Effects

The next subsystem was used to explore the effect of astrocytes on amyloid fiber toxicity. We incorporated the following properties of astrocytes: (a) uptake of IL-1B and activation to receptive and/or motile, (b) motion towards nearby fibrous deposits and (c) ability to wall-off or seal-off a region, represented by the decreased diffusivity of chemicals across "barriers" created by the astrocytes: dark gray areas surrounding a plaque in Fig. 6 denote such barriers, i.e. sites of reduced diffusion for soluble species. Such regions tend to hold elevated concentrations of chemicals, though the seal is generally somewhat permeable.

Results can be summarized as follows. (a) Astrocytes tend to cluster at the periphery of plaques but some remain scattered throughout; In many cases, some amyloid and other soluble substances can leak out through the astrocytic seals. This leads to a low level of fiber in the region surrounding the affected areas. (b) Variability with a given set of parameters arises, as before, from the number of secondary amyloid sources, the timing of those new sources, how long they last, and their proximity to one another. (c) Results are strongly affected by the following factors: probability of formation of new amyloid sources, persistence of those sources (depends on the sensitivity of the neurons: if death is rapid, the progression of the pathology is not as wide), and to a lesser extent on the effectiveness of the astrocyte barriers.

Typical shapes of plaques are shown in Fig. 7. In parts (a)–(d) fast neuronal dynamics, and in parts (e) and (f) slow neuronal health dynamics were assumed. The figures are qualitatively similar, and their time courses are shown in Fig. 8. In extreme cases, there is no new source created, and the plaque is quite small [see Fig. 7(d)], while in other cases, the new sources close to the original one lead to massive and lethal fibrous deposits [Fig. 7(b)]. The variability in the average health of neurons in various runs is also illustrated in Fig. 8.

We experimented with a variety of parameter settings. The evolution of a developing plaque in the presence of astrocytes for one set is shown in Fig. 10. The final shape resembles some plaque

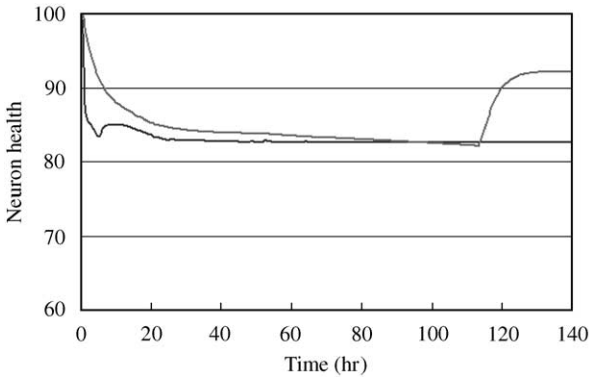

FIG. 12. A comparison between fast and slow neuron health dynamics in the case that IL-6 is the only toxic substance affecting neurons. This run shows time on a scale of hours over a period of almost 6 days. Two runs are shown in which the only difference is the timescale of neuron health dynamics. In the slow run we used $e_C = 0.600$ for IL-6 effects on health and $r = 0.0060$ for the health recovery rate. In the fast run, we used $e_C = 12.5$, $r = 0.1$: (——) fast; (——) slow.

shapes in AD shown in Fig. 1 and in Itakagi *et al.* (1989), Akiyama *et al.* (1999) and others. The central plaque is relatively self-contained. However, smaller plaques tend to sprout off the central one, in places where the astrocyte seal has imperfections (Fig. 10).

Toxicity of an Astrocyte Product

The next investigation explored the hypothesis that astrocytic secretions, rather than amyloid lead to neuronal toxicity. We assumed that the rate of secretion of some deleterious astrocyte product depends on the fraction of IL-1B receptors on the astrocyte that are bound to IL-1B. As a result, proximity of astrocytes to activated microglia became highly significant in determining whether and to what extent neurotoxicity occurs.

Two substances secreted by astrocytes are represented explicitly in the simulation. For default parameter settings, we have based the main attributes of these simulated chemicals on characteristics of the cytokines, IL-6 and TNF-alpha (Fig. 2), but this is not to indicate any claim that either of these cytokines is directly neurotoxic. (Evidence is controversial in both cases.) Qualitative spatio-temporal results described here should be closely related to results obtained with any other small (15–30 kDa) diffusible astrocytic peptide, with similar rates of uptake or secretion. (Exploration of effects of larger or smaller substances can be accommodated easily in the simulation by adjusting the appropriate rates of diffusion, secretion, uptake, and/or impact on neuronal health.)

We found that several representative scenarios occurred, including (a) stress of a wide zone followed by death in some small region. In cases where amyloid sources were then extinguished, there followed progressive recovery in all but the dead core. The average neuronal health in such runs decreased, achieved some minimum, and then increased by partial recovery. Figures 11 and 12 illustrate a representative example of this type. (b) In some cases, the initial wave of death does not remove all amyloid sources, and a perpetually stressed region surrounds one or more dead cores (not shown). The numbers and sizes of such dead regions depend on the number of amyloid sources that were formed. (c) Persistence of a perpetually stressed area with no net recovery and no net death (not shown). This occurred in cases where steady-state concentrations of the astrocyte toxin were not high enough to kill neurons outright and amyloid sources in the region continued to be active.

In all cases, the pathology has different dynamics under the assumption that death is caused solely by soluble substances that diffuse rapidly in the region. Unlike fibrous amyloid, which persists over extended periods of time, such factors are present only so long as glial cells are activated by stimuli (in this case amyloid) to keep up production. This affects the recovery process, and (by virtue of more even spread) causes necrotic areas to be more symmetrically distributed.

COMPARISON WITH OBSERVED PLAQUES

In this study, our primary interest is a comparison of gross features of the morphology of plaques that might result from one or another set of hypotheses about effects of amyloid, glial cells, and factors produced by such cells. Many quantitative details of such interactions were gathered and incorporated in the simulation, though the number of unknown parameter

values still limits our ability to describe the process in detail. At this stage of the investigation, detailed quantitative comparison of simulated plaques to real plaques is still somewhat premature.

Hyman *et al.* (1995) computed size distributions of plaques in an AD patient, and reported a log-normal distribution. We performed some preliminary quantitative estimates of plaque size distributions (for parameter sets corresponding to Figs 7 and 8) and compared results with those of Hyman *et al.* The comparison is shown in Fig. 9). Here the relative proportions (vertical axis) of plaques of various sizes (horizontal axis, in multiples of $100\,\mu m^2$) have been tabulated for a set of 50 simulations, each run for 400 time steps (dark bars). We defined the "size" of a plaque as the area occupied by high fiber concentrations that corresponded to killing zones, i.e. to black squares in the final state of the region. Shown on the same histogram (light bars) are the data from Hyman *et al.*

Our results for the given set of parameters are qualitatively similar, with most numerous plaques in the $100\,\mu m^2$ size category, though some differences are notable. In particular, shown grouped in the largest category are all cases in which significantly larger plaques occurred, stemming from coalescence of effects of multiple amyloid sources in close proximity. It is still unclear what prevents such large plaques from forming in the real AD brain, though we might speculate that other processes tending to limit the production of amyloid, or to more effectively sealing areas in proximity of a source may be at play.

Discussion

While still at a preliminary stage, the simulation described here has provided a number of insights and results. We highlight these briefly below.

1. The result of a stimulus depends on a balance between competing effects. Clearly, the balance between production and uptake of substances determines whether the levels of injurious factors will build up to dangerous levels. Some removal rates (e.g. of amyloid by microglia, of cytokines by various cells) tends to saturate due to receptor kinetics, and can be overwhelmed and pushed to toxic levels by high rates of production. Protective and injurious effects of cells also compete: for example, microglia remove amyloid, reducing local stress, but also secrete IL-1B that promotes new amyloid sources. Astocytes wall off a region to help cap the spread of toxicity, but they also contribute to the inflammation by secreting cytokines. While these results are not surprising, they lend support to many of the hypotheses current in the field (see, for example, McGeer & McGeer 1995, 1998a, b, 1999). Since the unfolding early events in the development of AD cannot be investigated easily *in vivo* by current techniques, the simulation can fill in gaps between known or hypothesized interactions and downstream consequences.

2. There are feedbacks in the system that can exacerbate pathology. One important feedback is the effect of microglial IL-1B on new sources of neuronal amyloid, and on a heightening of the toxic load. This seems reasonable with hindsight, particularly in the context of the analogy with spread of infections in other modeling contexts. However, the overriding importance of the parameter that controls this feedback was not at all evident to us before undertaking extensive experimentation and parameter sensitivity.

3. There are delays in the system, e.g. between the initiation of the stimulus and arrival of microglia, between the production of cytokines and activation of astrocytes, between the uptake of cytokines and the death of neurons. The extent to which this delay affects outcomes became apparent only after experimenting with the simulation. This means that there is some time when interventions could, in principle, reverse the process and prevent massive death of neurons. Conversely, once an inflammatory process is initiated, there is a time delay in halting it, even if the irritant is removed. This delay results from the time it takes for the inflammatory chemicals to be removed, and the activated immune-like cells to return to a quiescent (non-secreting) state.

4. For a given parameter set, results are quite variable, and randomness plays an important

role. In some cases, the outcome on health of neurons can differ by 50% or more in parallel runs. There are several causes for variability in the runs, including (a) stochastic aspects of cell motion (b) random initial distributions of cells, and (in some cases) fiber seeds, (c) proximity of nascent plaques to one another or to groups of astrocytes that affect activation levels of those astrocytes (d) random component of new amyloid source initiations. All these effects are likely to play a role in a real biological setting, where many other sources of individual cell variability might also be important.

5. Among the variable factors is the dichotomy between cases in which inflammation persists with no resolution over extended periods vs. cases in which there is a finite transient, with some lost tissue surrounded by a region of nearly full recovery.

6. The simulation reveals the importance of spatio-temporal effects. These include (a) the importance of relative placement of cells with respect to other cell types or to amyloid sources. (e.g. we noted that astrocytes behave differently away from microglia, even when they are in proximity of an amyloid source). (b) The importance of relative time-scale of neuronal degeneration and other processes that lead to that degeneration. We saw that the conditions that pre-dispose neurons to die can become irreversible long before neurons react, and this tends to cause severe eventual outcomes, in contrast to local limited death in other cases. (c) Changes in material properties caused by astrocytes in proximity of a plaque result in trapping of substances in a localized way. This affects the way that plaques develop. (d) Distinct patterns of mortality are noted when the factors causing stress of neurons are local and persistent (such as amyloid deposits) vs. soluble, labile, and rapidly diffusing (such as cytokines or other substances). Note that none of these effects were "built in" or pre-assumed, but rather emerged from the underlying spatio-temporal interactions.

Aside from these observations, the simulation is also a useful tool for exploring the sensitivity of the system to a variety of parameters. As noted, by shifting the balance towards production or towards removal of any injurious chemical factor, one can produce outcomes that bias the results towards full health or full mortality. The relative rates of recovery and injury similarly affect the outcome as expected: once a threshold is crossed, the system cannot recover from an insult that, in other circumstances, might be inconsequential. This situation may reflect real biological differences between those people susceptible to AD and those who are not: some slight change that shifts the balance of effects would suffice to produce the fatal pathology.

Less intuitively clear is the observation that severity of the disease need not correlate positively with sensitivity of neurons to amyloid fibers. Indeed, we found that when amyloid fibers are highly and rapidly toxic, neurons close to a source of amyloid die so quickly, that the process is halted before the amyloid deposits spread. Even if numerous amyloid sources are present, this results in only small regions where neurons have died, and eliminates the sources rapidly. This means that inflammation has little opportunity to take hold. In the simulation, neuronal death is the main factor controlling the persistence time of the amyloid sources. This may or may not be the case in real neurons, and factors that govern the amount of amyloid production, and its rate of fibrillization may be equally, or more important.

One parameter that had an interesting and highly significant effect is the fraction of neurons capable of producing new amyloid sources when stimulated by IL-1B. When this fraction is low (in our case, below 0.2%), the system response stems from one stimulus, present at initiation. This is analogous to gradual outward spread of an epidemic from a single site of infection, or gradual spread of a fire from a single ignited source. The spread of such infections tends to be limited to the perimeter of the affected region, where contact with a susceptible region occurs, or to the internal "volume" of the region, given a porous or fractal interior structure (Cruz *et al.*, 1997). This contrasts with pandemics in which secondary sites of infection arise or fires whose sparks ignite new areas. As a result of such secondary sites, the process of infection can grow exponentially (at least while susceptible areas

remain) instead of simply spreading "radially" outwards.

A similar phenomenon occurs when the fraction of neurons capable of producing new amyloid sources rises slightly to 0.4%: we found that in such cases, the initial stimulus nearly always creates one or more secondary sources. (Significantly, this can occur even after the original amyloid source is extinguished, as the accumulated microglial IL-1B that triggers the new sources takes time to decay.) This causes significant worsening of the situation, either by feeding massive growth of one expanding plaque (when the amyloid sources are close together) or by spawning new plaques in adjoining regions. The fraction of neurons that die is usually much greater in such cases.

It is worth remarking that this type of sharp threshold is similar to a bifurcation that occurs when the *basic reproductive rate*, r of an infection increases above 1 (r is the number of secondary infections in a susceptible population caused by a single infected person during the time course of the infection). As argued here, a similar parameter in our model represents the ability of the inflammatory stimulus to replicate other stimuli before being eliminated by the response.

LIMITATIONS

In considering the results, a number of limitations of the current model must be appreciated. We list some of the limitations below.

(1) To allow our simulation to be run online interactively (www.math.ubc.ca/$\sim$ais), it has been written in Java, a framework with limited computational speed and memory capabilities. We have simulated two spatial dimensions to suit these computational resources, though this is clearly a drastic simplification. Comments about differences between diffusion in 2D and 3D are given in the appendix. Basically, the time associated with a diffusion process (or, analogously, the distance through which diffusion has an effect over a given time span) can depend on dimensionality. (2) Only a few key interacting parts are modeled explicitly. The other effects (chemical factors, environmental and genetic pre-disposition) are treated as variations in basic parameter values. We may be missing other dynamical phenomena by our omissions. (3) Finding a reasonable set of biological parameter values is the single biggest challenge. After extensive research, this set is incomplete (20–30% missing or unknown, including rates of decay of neuronal health). Those parameters we could estimate (e.g. receptor binding, secretion rates, etc.) are pertinent to a variety of species under various conditions (*in vivo*, *in vitro*, with distinct treatments) and are suspect, to say the least. This difficulty is not just a problem we had to contend with: rather, it is an indication of one of the grand challenges facing *in silico* modeling in general. This challenge is far from being addressed and leads to natural skepticism about validity of the results of such work. It remains to be seen to what extent such challenges can be overcome, even with close work coupling experimental research and theoretical models. (4) The neuro-inflammatory hypothesis, and its details are still controversial, with wide disagreement in the scientific community about basic facts. The simulation would have to be changed as new information is gathered. (5) Even in this simplified system, the set of parameters is quite large. This makes it difficult to explore parameter space and find all the relevant transitions in behavior. This is a second "grand challenge" facing the new biology: how to understand the complex behavior of large interacting networks, even when their parts are well characterized. The challenge is even greater when many parts of the interacting network are unknown. (6) The time-scale for health deterioration in neurons may be faster in the simulation than in reality. While we have checked that most interesting regimes can be obtained on a slower time-scale by suitable scaling of the parameters, this aspect should be studied further as more information about neuronal degeneration dynamics *in vivo* is gathered.

Future work will be aimed at addressing some of the above limitations. In particular, we plan to investigate more realistic neuronal health kinetics based on intracellular events, including other chemical intermediates explicitly, study the process on a longer time-scale, with a more faithful replication of the time course of AD, and

design experiments to measure some of the uncertain parameters. We will then be in a position to test interventions and potential drug target designs.

The authors were supported by NSERC (Canada) funds to LEK and by MITACS NCE funds. We were also funded for 1 year by In Silico Biosciences (R Carr, Pres.). The following people provided valuable comments: Dr P. McGeer, Dr C. Shaw, Dr S. Maree, Dr M. Labecki, M. Luca, J. McEachern. Thanks to A. Klegeris, A. Chavez-Ross, J. McEachern, M. Luca and T. Wong for help with references, bibliography, literature surveys, figures, etc. We extend special thanks to Claudia Schwab for providing images for Fig. 1.

REFERENCES

Akiyama, H., *et al*. (The Neuroinflammation working group) (1999). Inflammation and Alzheimer's disease. *Neurobiol. Aging.* **21,** 383–421.

Ard, M. D., Cole, G. M., Wei, J., Mehrle, A. P. & Fratkin, J. D. (1996). Scavenging of Alzheimer's amyloid beta-protein by microglia in culture. *J. Neurosci. Res*. **43,** 190–202.

Benes, F. M., Reifel, J. L., Majocha, R. E. & Marotta, C. A. (1989). Evidence for a diffusional model of Alzheimer's amyloid A4 beta amyloid deposition during neurotic plaque formation. *Neuroscience* **33,** 483–488.

Benjamin, D., Wormsley, S. & Dower, S. K. (1990). Heterogeneity in interleukin (IL)-1 receptors expressed on human B cell lines. Differences in the molecular properties of IL-1 alpha and IL-1 beta binding sites. *J. Biol. Chem.* **265,** 9943–9951.

Benveniste, E. N., Tang, L. P. & Law, R. M. (1995). Differential regulation of astrocyte TNF-alpha expression by the cytokines TGF-beta, IL-6 and IL-10. Int. *J. Dev. Neurosci*. **13,** 341–349.

Bocci, V. (1998) Central nervous system toxicity of interferons and other cytokines, *J Biol. Regul. Homeost. Agents* **2,** 107–118.

Brugg, B., Dubreiul, Y. L., Huber, G., Wollman, E. E., Delhaye-Bouchaud, N. & Mariani, J. (1995). Inflammatory processes induce beta-amyloid precursor protein changes in mouse brain, *Proc. Natl Acad. Sci. U.S.A.* **92,** 3032–3035.

Bush, A. I., Pettingell, W. H., Multhaup, G., Paradis, M. D., Vonsattel, J.-P, Gusella, J. F., Beyreuther, K., Masters, C. L. & Tanzi, R. E. (1994). Rapid induction of Alzheimer A-beta amyloid formation by zinc. *Science* **265,** 1464–1467.

Buxbaum, J. D., Oishi, M., Chen, H. I., Pinkas-Kramarski, R., Jaffe, E. A., Gandy, S. E. & Greengard P. (1992). Cholinergic agonists and interleukin 1 regulate processing and secretion of the Alzheimer's beta A4 amyloid protein precursor. *Proc. Natl Acad. Sci.* U.S.A. **89,** 10075–10078.

Cai, X.-D., Golde, T. E. & Younkin, S. G. (1993). Release of excess amyloid beta protein from a mutant amyloid beta protein precursor. *Science* (Washington, DC). **259,** 514–516.

Carlson, N. G., Wieggel, W. A., Chen, J., Bacchi, A., Rogers, S. W. & Gahring, L.C. (1999). Inflammatory cytokines IL-1 alpha, IL-1 beta, IL-6, and TNF-alpha impart neuroprotection to an excitotoxin through distinct pathways, *J. Immunol.* **163,** 3963–3968.

Chao, C. C., Hu, S., Ehrlich, L. & Peterson, P. K. (1995). Interleukin-1 and tumor necrosis factor-alpha synergistically mediate neurotoxicity: involvement of nitric oxide and of N-methyl-D-aspartate receptors. *Brain Behav. Immun.* **9,** 355–365.

Cheng, B., Christakos, S. & Mattson, M. P. (1994). Tumor necrosis factors protect neurons against metabolic-excitotoxic insults and promote maintenance of calcium homeostasis. *Neuron* **12,** 139–153.

Christie, R. H., Bacskai, B. J., Zipfel, W. R., Williams, R. M., Kajdasz, S. T., Webb, W. W. & Hyman, B. T. (2001). Growth arrest of individual senile plaques in a model of Alzheimer's disease observed by in vivo multiphoton microscopy. *J. Neurosci*. **21,** 858–864.

Clarke, G., Collins, R. A., Leavitt, B. R., Andrews, D. F., Hayden, M. R., Lumsden, C. J. & Mcinnes, R. R. (2000). A one-hit model of cell death in inherited neuronal degenerations. *Nature* **406,** 195–199.

Clarke, G., Lumsden, C. J. & McInnes, R. R. (2001). Inherited neurodegenerative diseases: the one-hit model of neurodegeneration. *Hum. Mol. Genet*. **10,** 1–7.

Come, J. H., Fraser, P. E. & Lansbury Jr., P. T. (1993). A kinetic model for amyloid formation in the prion Diseases: Importance of seeding, *PNAS* **90,** 5959–5963.

Cruz, L., Urbanc, B., Buldyrev, S. V., Christie, R., Gmez-Isla, T., Havlin, S., McNamara, M., Stanley, H. E. & Hyman, B. T. (1997). Aggregation and disaggregation of senile plaques in Alzheimer disease. *Proc. Natl Acad. Sci. U.S.A.* **94,** 7612–7616.

Davis, J. B., McMurray, H. F. & Schubert, D. (1992). The amyloid beta-protein of Alzheimer's disease is chemotactic for mononuclear phagocytes. *Biochem. Biophys. Res. Commun.* **189,** 1096–1100.

Ding, A. H., Sanchez, E., Srimal, S. & Nathan, C. F. (1989). Macrophages rapidly internalize their tumor necrosis factor receptors in response to bacterial lipopolysaccharide. *J. Biol. Chem*. **264,** 3924–3929.

Donnelly, R. J., Freidhoff, A. J., Beer, B., Blume, A. J. & Vitek, M. P. (1990) Interleukin-1 stimulates the beta-amyloid precursor protein promoter. *Cell Mol. Neurobiol.* **10,** 485–495.

Dripps, D. J., Brandhuber, B. J., Thompson, R. C. & Eisenberg, S. P. (1991). Interleukin-1 (IL-1) receptor antagonist binds to the 80-kDa IL-1 receptor but does not initiate IL-1 signal transduction. *J. Biol. Chem*. **266,** 10331–10336.

Eddershaw, P. J., Beresford, A. P. & Bayliss, M. K. (2000). ADME/PK as part of a rational approach to drug discovery. *Drug Discovery Today* **5,** 409–414.

Edelstein-Keshet, L. (1998). *Mathematical Models in Biology*. New York, McGraw Hill.

Ekinci, F. J., Linsley, M.-D. & Shea, T. B. (2000). Beta-Amyloid-induced calcium influx induces apoptosis in culture by oxidative stress rather than tau phosphorylation. *Mol. Brain Res*. **76,** 389–395.

El Khoury, J., Hickman, S. E., Thomas, C. A., Cao, L., Silverstein, S. C. & Loike, J. D. (1996). Scavenger receptor-mediated adhesion of microglia to beta-Amyloid fibrils. *Nature* **382,** 716–719.

Endy, D., You, L., Yin, J. & Molineux, I. J. (2000). Computation, prediction, and experimental tests of fitness for bacteriophage T7 mutants with permuted genomes. *Proc. Natl Acad. Sci. U.S.A.* **97,** 5375–5380.

Fassbender, K., Simmons, M., Bergmann, C., Stroick, M., Lutjohann, D., Keller, P., Runz, H., Kuhl.S., Bertsch, T., Von Bergmann, K., Hennerici, M., Beyreuther, K. & Hartmann, T. (2001). Simvastatin strongly reduces levels of Alzheimer's disease Beta-amyloid peptides A beta-42 and A beta-40 in vitro and in vivo. *PNAS*, online edition.

Fiala, M., Zhang, L., Gan, X., Sherry, B., Taub, D., Graves, M. C., Hama, S., Way, D., Weinand, M., Witte, M., Lorton, D., Kuo, Y. M. & Roher, A. E. (1998). Amyloid-beta induces chemokine secretion and monocyte migration across human blood-brain barrier model. *Mol. Med.* **4,** 480–489.

Fink, C. C., Slepchenko, B., Moraru, I. I., Watras, J., Schaff, J. & Loew, L. M. (2000). An image-based model of calcium waves in differentiated neuroblastoma cells. *Biophys. J.* **79,** 163–183.

Forloni, G., Demichelli, F., Giorgi, S., Bendotti, C. & Angretti, N. (1992). Expression of amyloid precursor protein mRNAs in endothelial, neuronal, and glial cells: modulation by interleukin-1. *Brain Res. Mol. Brain. Res.* **16,** 128–134.

Gelbard, H. A., Dzenko, K. A., DiLoreto, D., Del Cerro, C., Del Cerro, M. & Epstein, L.G. (1993). Neurotoxic effects of tumor necrosis factor alpha in primary human neuronal cultures are mediated by activation of the glutamate AMPA receptor subtype: implications for AIDS neuropathogenesis. *Dev. Neurosci.* **15,** 417–422.

Giulian, D., Li, J., Leara, B. & Keenen, C. (1994). Phagocytic microglia release cytokines and cytotoxins that regulate the survival of astrocytes and neurons in culture, *Neurochem. Int.* **25,** 227–233.

Godard, A., Heymann, D., Raher, S., Anegon, I., Peyrat, M. A., Le, Mauff, B., Mouray, E., Gregoire, M., Virdee, K., Soulillou, J. P., Moreau, J. F. & Jacques, Y. (1992). High and low affinity receptors for human interleukin for DA cells/leukemia inhibitory factor on human cells. Molecular characterization and cellular distribution. *J. Biol. Chem.* **267,** 3214–3222.

Goodhill, G. J. (1997). Diffusion in axon guidance. *Eur. J. Neurosc.* **9,** 1414–1421.

Gray, C. P. & Keck, W. (1999). Bacterial targets and antibiotics: genome-based drug discovery. *Cell. Mol. Life Sci.* **56,** 779–787.

Griffin, W. S. T., Sheng, J. G. & Mrak, R. E. (1996). Inflammatory pathways, In: Molecular Mechanisms of Dementia: (Wasco, W., Tanzi, R. E. eds). Totowa, NJ: Humana Press.

Griffin, W. S. T., Sheng, J. G., Royston, M. C., Gentleman, S. M., McKenzie, J. E., Graham, D. I., Roberts, G. W. & Mrak, R. E. (1998). Glial-neuronal interactions in Alzheimer's disease: the potential role of a 'cytokine cycle' in disease progression. *Brain Pathol.* **8,** 65–72.

Hammacher, A., Simpson, R. J. & Nice, E. C. (1996). The interleukin-6 (IL-6) partial antagonist (Q159E,T162P) IL-6 interacts with the IL-6 receptor and gp130 but fails to induce a stable hexameric receptor complex. *J. Biol. Chem.* **271,** 5464–5473.

Hardt, S. L. (1981). The diffusion transit times: a simple derivation. *Bull. Math. Biol.* **43,** 89–99.

Horuk, R., Huang, J. J., Covington, M. & Newton, R. C. (1987). A biochemical and kinetic analysis of the interleukin-1 receptor. Evidence for differences in molecular properties of IL-1 receptors. *J. Biol. Chem.* **262,** 16275–16278.

Hu, J. & Van Eldik, L. J. (1999). Glial-derived proteins activate cultured astrocytes and enhance beta amyloid-induced glial activation. *Brain Res.* **842,** 46–54.

Huang, X., Atwood, C. S., Hartshorn, M. A., Multhaup, G., Goldstein, L. E., Scarpa, R. C., Cuajungco, M. P., Gray, D. N., Lim, J., Moir, R. D., Tanzi, R. E. & Bush, A. I. (1999a). The A peptide of Alzheimer's disease directly produces hydrogen peroxide through metal ion reduction. *Biochemistry*. **38,** 7609–7616.

Huang, X., Cuajungco, M. P., Atwood, C. S., Hartshorn, M. A., Tyndall, J. D. A., Hanson, G. R., Stokes, K. C., Leopold, M., Multhaup, G., Goldstein, L. E., Scarpa, R. C., Saunders, A. J., Lim, J., Moir, R. D., Glabe, C., Bowden, E. F., Masters, C. L., Fairlie, D. P., Tanzi, R. E. & Bush, A. I. (1999b). Cu(II) potentiation of Alzheimer a neurotoxicity. Correlation with cell-free hydrogen peroxide production and metal reduction. *J. Biol. Chem.* **274,** 37 111–37 116.

Hyman, B. T., West, H. L., Rebeck, G. W., Buldyrev, S. V., Mantegna, R. N., Ukleja, M., Havlin S. & Stanley, H. E. (1995). Quantitative analysis of senile plaques in Alzheimer disease: observation of log-normal size distribution and molecular Epidemiology of differences associated with apolipoprotein E genotype and trisomy 21 (Down syndrome). *PNAS* **92,** 3586–3590.

Itagaki, S., McGeer, P. L., Akiyama, H., Zhu, S. & Selkoe, D. (1989). Relationship of microglia and astrocytes to amyloid deposits of Alzheimer disease. *J. Neuroimmunol.* **24,** 173–182.

Jeohn, G. H., Kong, L. Y., Wilson, B., Hudson, P. & Hong, J. S. (1998). Synergistic neurotoxic effects of combined treatments with cytokines in murine primary mixed neuron/glia cultures. *J Neuroimmunol.* **85,** 1–10.

Kim, W. G., Mohney, R. P., Wilson, B., Jeohn, G. H., Liu, B. & Hong, J. S. (2000). Regional difference in susceptibility to lipopolysaccharide-induced neurotoxicity in the rat brain: role of microglia. *J. Neurosci.* **20,** 6309–6316.

Klegeris, A., Walker, D. G. & McGeer, P. L. (1999). Toxicity of human THP-1 monocytic cells towards neuron-like cells is reduced by nonsteroidal anti-inflammatory drugs (NSAIDS). *Neuropharmacology* **38,** 1017–1025.

Kornyei, Z., Czirok, A., Vicsek, T. & Madarasz, E. (2000). Proliferative and migratory responses of astrocytes to in vitro injury. *J. Neurosci. Res.* **61,** 421–429.

Lee, S. C., Liu, W., Dickson, D. W., Brosnan, C. F. & Berman, J. W. (1993). Cytokine production by human

fetal microglia and astrocytes, differential induction by lipopolysaccharide and IL-1-beta. *J. Immunol*. **150,** 2659–2667.

Ma, T. C. & Zhu, X. (2000). Neurotoxic effects of interleukin-6 and sodium nitroprusside on cultured rat hippocampal neurons. *Arzneimittelforschung* **50,** 512–514.

Mazel, T., Simonova, Z. & Sykova, E. (1998). Diffusion heterogeneity and anisotropy in rat hippocampus. *Neuroreport*. **9,** 1299–1304.

Michishita, M., Yoshida, Y., Uchino, H. & Nagata, K. (1990). Induction of tumor necrosis factor-alpha and its receptors during differentiation in myeloid leukemic cells along the monocytic pathway. A possible regulatory mechanism for TNF-alpha production. *J. Biol. Chem*. **265,** 8751–8759.

McGeer, E. G. & McGeer, P. L. (1999). Brain inflammation in Alzheimer disease and the therapeutic implications. *Curr. Pharmaceut. Des*. **5,** 821–836.

McGeer, P. L. & McGeer, E. G. (1998a). Mechanisms of cell death in Alzheimer disease—immunopathology. *J. Neural Transmission*. (Suppl.) **54,** 159–166.

McGeer, E. G. & McGeer, P. L. (1998b). The importance of inflammatory mechanisms in Alzheimer disease. *Exp. Gerontol*. **33,** 371–378.

McGeer, P. L. & McGeer, E. G. (1995). The inflammatory response system of brain: implications for therapy of Alzheimer and other neurodegenerative diseases. *Brain. Res. Brain. Res. Rev.* **21,** 195–218.

McLean, C. A., Cherny, R. A., Fraser, F. W., Fuller, S. J., Smith, M. J., Beyreuther, K., Bush, A. I. & Masters, C. L. (1999). Soluble pool of Abeta amyloid as a determinant of severity of neurodegeneration in Alzheimer's disease. *Ann. Neurol*. **46,** 860–866.

Michaelis, M. L., Ranciat, N., Chen, Y., Bechtel, M., Ragan, R., Hepperle, M., Liu, Y. & Georg, G. (1998). Protection against beta-amyloid toxicity in primary neurons by paclitaxel (Taxol). *J. Neurochem*. **70,** 1623–1627.

Moghe, P. V., Nelson, R. D. & Tranquillo, R. T. (1995). Cytokine-stimulated chemotaxis of human neutrophils in a 3-D conjoined fibrin gel assay. *J. Immunol. Methods* **180,** 193–211.

Moir, R. D., Atwood, C. S., Romano, D. M., Laurans, M. H., Huang, X., Bush, A. I., Smith, J. D. & Tanzi, R. E. (1999). Differential effects of apolipoprotein E isoforms on metal-induced aggregation of A using physiological concentrations. *Biochemistry* **38,** 4595–4603.

Mrak, R. E., Sheng, J. G. & Griffin, W. S. T. (1995). Glial cytokines in Alzheimer's disease: review and pathogenic implications. *Hum. Pathol*. **26,** 816–823.

Mrak, R. E., Sheng, J. G. & Griffin, W. S. T. (2000). Glial cytokines in neurodegenerative conditions. In: *Neuro-Immune Interactions in Neurologic and Psychiatric Disorders* (Patterson, P. H., Kordon, C., Christen, Y. eds). Berlin Heidelberg: Springer-Verlag.

Nicholson, C. & Sykova, E. (1998). Extracellular space structure revealed by diffusion analysis. *Trends in Neurosciences* **21**, 207–215.

Nolte, C., Moeller, T., Walter, T. & Kettenmann, H. (1996). Complement 5a controls motility of murine microglial cells in vitro via activation of an inhibitory G-protein and the rearrangement of the actin cytoskeleton. *Neuroscience* **73,** 1091–1107.

Nolte, C., Kirchhoff, F. & Kettenmann, H. (1997). Epidermal growth factor is a motility factor for microglial cells in vitro: evidence for EGF receptor expression. *Eur. J. Neurosc.* **9,** 1690–1698.

Norris, D. A., Leesman, G. D., Sinko, P. J. & Grass, G. M. (2000). Development of predictive pharmacokinetic simulation models for drug discovery. *J. Control. Release* **65,** 55–62.

Palsson, B. (2000). The challenges of *in silico* biology. *Nat. Biotechnol*. **18,** 1147–1150.

Pennica, D., Lam, V. T., Mize, N. K., Weber, R. F., Lewis, M., Fendly, B. M., Lipari, M. T. & Goeddel, D. V. (1992). Biochemical properties of the 75-kDa tumor necrosis factor receptor. Characterization of ligand binding, internalization, and receptor phosphorylation. *J. Biol. Chem.* **267,** 21 172–21 178.

Press, W. H., Flannery, B. P., Teukolsky, S. A. & Vetterling, W. T. (1988). *Numerical Recipes in C: the Art of Scientific Computing*. Cambridge: Cambridge Press.

Rivero, M. A., Tranquillo, R. T., Buettner, H. M. & Lauffenburger, D. A. (1989). Transport models for chemotactic cell populations based on individual cell behaviour. *Chem. Eng. Sci.* **44,** 2881–2897.

Schaff, J., Fink, C., Slepchenko, B., Carson, J. & Loew, L. (1997). A general computational framework for modeling cellular structure and function. *Biophys. J*. **73,** 1135–1146.

Selkoe, D. J. (1991). Amyloid protein and Alzheimer's disease. *Sci. Am*. **265,** 68–78.

Shaffer, L. M., Dority, M. D., Gupta-Bansal, R., Frederickson, R. C., Younkin, S. G., Brunden, K. R. (1995). Amyloid beta protein (A beta) removal by neuroglial cells in culture. *Neurobiol. Aging* **16,** 737–745.

Sheng, J. G., Ito, K., Skinner, R. D., Mrak, R. E., Rovnaghi, C. R., Van Eldik, L. J., Griffin, W. S. T. (1996). *In vivo* and *In vitro* evidence supporting a role for the inflammatory cytokine interleukin-1 as a driving force in Alzheimer pathogenesis. *Neurobiol. Aging* **17,** 761–766.

Sheng, J. G., Mrak, R. E. & Griffin, W. S. T. (1997). Enlarged and phagocytic, but not primed, interleukin-1alpha immunoreactive microglia increase with age in normal human brain. *Acta Neuropathol* **95,** 229–234.

Stoll, G., Jander, S. & Schroeter, M. (2000). Cytokines in CNS disorders: neurotoxicity versus neuroprotection. *J. Neural. Transm*. (Suppl) **59,** 81–89.

Strikwerda, J. C. (1989). *Finite Dierence Schemes and Partial Dierential Equations*. Pacific Grove, CA: Wadsworth and Brooks/Cole Advanced Books and Software.

Sykova, E. (1997). The extracellular space in the CNS: its regulation, volume, and geometry in normal and pathological neuronal function. *Neuroscientist* **3,** 28–41.

Sykova, E., Mazel, T. & Simonova, Z. (1998). Diffusion constraints and neuron-glia interaction during aging. *Exp. Gerontol*. **33,** 837–851.

Streit, W. J. & Kincaid-Colton, C. A. (1995). The Brain's immune system, *Sci. Am.* 273, 54–61.

Tarkowski, E., Blennow, K., Wallin, A., Tarkowski, A. (1999). Intracerebral production of tumor necrosis factor-alpha, a local neuroprotective agent, in Alzheimer

disease and vascular dementia. *J Clin. Immunol*. **19,** 223–230.

Tomita, M., Hashimoto, K., Takahashi, K., Shimizu, T. S., Matsuzaki, Y., Miyoshi, F., Saito, K., Tanida, S., Yugi, K., Venter, J. C. & Hutchison III, C. A. (1999). E-CELL: software environment for whole-cell simulation. *Bioinformatics* **15,** 72–84.

Urbanc, B., Buldyrev, S. V., Christie, R., Gomez-Isla, T., Havlin, S., McNamara, M., Stanley, H. E. & Hyman, B. T. (1997). Aggregation and disaggregation of senile plaques in Alzheimer disease. *Proc. Natl Acad. Sci. U.S.A.* **94,** 7612–7616.

Urbanc, B., Cruz, L., Buldyrev, S. V., Havlin, S., Irizarry, M. C., Stanley, H. E. & Hyman, B. T. (1999). Dynamics of plaque formation in Alzheimer's disease. *Biophys. J.* **76,** 1330–1334.

Van Wagoner, N. J., Oh, J. W., Repovic, P. & Benveniste, E. N. (1999). Interleukin-6 (IL-6) production by astrocytes: autocrine regulation by IL-6 and the soluble IL-6 receptor. *J. Neurosci* **19,** 5236–5244.

von Zahn, J., Moeller, T., Kettenmann, H. & Nolte, C. (1997). Microglial phagocytosis is modulated by pro-and anti-inflammatory cytokines. *Neuroreport* **8,** 3851–3856.

Yamaguchi, M., Michishita, M., Hirayoshi, K., Yasukawa, K., Okuma, M. & Nagata, K. (1992) Down-regulation of interleukin 6 receptors of mouse myelomonocytic leukemic cells by leukemia inhibitory factor. *J. Biol. Chem*. **267,** 22 035–22 042.

Appendix

TIME STEPPING AND SPATIAL RESOLUTION

A short time increment ($dt = 0.0125$ min) is used to compute chemical diffusion. A longer time increment ($DT = 0.5$ min) is used for calculating cell movement and transitions in the states of the cells. The region shown corresponds roughly to a square area of side length 400 μm, discretized into a 40×40 spatial grid.

CHEMICAL DIFFUSION COMPUTATIONS

Rates of diffusion of typical substances associated with AD were estimated from molecular sizes of the chemicals (see Table A1). The concentration of chemical in a grid space (i,j), denoted as $S^1_{i,j}$, is computed using an explicit numerical integration method based on the concentrations of the chemical in the previous time step, $S^0_{i,j}$. Choice of the explicit method was constrained by limitations on speed and memory available in a Java-based online application. In cases where the material properties of the region were not homogeneous, many numerical schemes (ordinarily adequate for uniform material properties) produce spurious results such as unrealistic amplification of concentrations. The numerical scheme was adjusted to preserve conservation principles. For example, we would compute flux *into* grid square *ij* from grid square $i-1$, j as follows:

$$J_{i-1,i}(i,j) = D_{ij}(c(i,j) - c(i-1,j))/\Delta x.$$

Note that the coefficients D_{ij} need not be constant in this formulation. We then calculate the new concentration in grid space *ij* using, for example

$$\Delta c(i,j) = \big[\big(J_{i-1,i} - J_{i,i+1}\big)/\Delta x + \big(J_{j-1,j} - J_{j,j+1}\big)/\Delta y + \sigma_{ij}\big]\Delta t.$$

The term σ_{ij} represents a source of chemical. Amyloid sources are stationary sites, whereas cytokine sources are cells (microglia, astrocytes) producing chemical at their current site of

Table A1

The diffusion coefficient of a soluble peptide scales approximately as a reciprocal of the cube root of its molecular weight (*Goodhill*, 1998, 1997), *a fact we used in estimating diffusion coefficients of all appropriate chemicals. For example, a* 0.3–0.5 *kDa peptide has a diffusion coefficient of approximately* $10^{-6}\,cm^2s^{-1} = 60\,\mu m^2 min^{-1}$

Molecule type	Molec. weight (kDa)	Diffusion coefficient	Effective diffusion coefficient ($\mu m^2\,min^{-1}$)	Reference
Amyloid-beta	3–4	$5 \times 10^{-7}\,cm^2s^{-1} = 3000\,\mu m^2min^{-1}$	1500	Goodhill (1997)
IL-1 beta	17	$3 \times 10^{-7}\,cm^2s^{-1} = 1800\,\mu m^2min^{-1}$	900	Goodhill (1997)
IL-6	26	$2.7 \times 10^{-7}\,cm^2s^{-1} = 1620\,\mu m^2min^{-1}$	810	Goodhill (1997); Moghe *et al.* (1995)
TNF-α	17	$3 \times 10^{-7}\,cm^2s^{-1} = 1800\,\mu m^2min^{-1}$	900	Goodhill (1997)

TABLE A2

Rates of secretion of cytokines by various cell types (*Lee et al.* 1993, *Fiala et al.*, 1998, *Van Wagoner et al.*, 1999) *are calculated as a local concentration change assuming that a* (*single*) *cell secretes substance into an adjoining volume of* $10\,\mu m^3$.

Type	Rate secreted per cell nM min^{-1}	Cell type
IL-1 beta	0.366	Microglia
IL-6	0.100	Astrocytes
TNF-alpha	0.049	Astrocytes

Note: For a substance of molecular weight M, the factor converting concentrations from pg ml^{-1} to nM is $c = [10^{-3}/(M)]$nM[pg $ml^{-1}]^{-1}$. If there are $\boldsymbol{n}$ cells secreting for $\boldsymbol{d}$ hr, the concentration change in the given volume will be $(10^9/60)$ $\boldsymbol{c}/(\boldsymbol{d}\,\boldsymbol{n})$ nM min^{-1} per cell.

occupancy. The formulation above ensures that flux of substance leaving one grid square matches with flux entering the adjoining square. This corrected such artifacts. (See further comments in the last section of this appendix.)

DIFFUSION IN TWO AND THREE DIMENSIONS

Diffusion depends on dimensionality (i.e. one, two, and three dimensions) in the following way. Diffusion over a distance x follows the relationship $\langle x^2 \rangle = q_i\, Dt$, where $\langle x^2 \rangle >$ is the mean-square displacement, t is the time taken, and the constant q_i has values 2, 4, or 6, for diffusion in one, two, or three dimensions. Similarly, the transit time to diffuse over a distance L has the form $\tau = (L^2/2D)\ f_i$ where the factor f_i is dimension-dependent. For example, in diffusion from a source to a target, setting $y = L/a$ where the diameter of the target is a and the distance to diffuse is L, it was shown by Hardt (1981) that the factor f_i is proportional to $\ln(y)$ in 2D, to y in 3D and independent of y in 1D. This can make a significant difference in the 2D and 3D cases when the ratio y is small.

MONTE-CARLO CELL MOTION AND STATE TRANSITIONS

Each moving particle ("agent") in the simulation represents cumulative effects of some number of actual cells. At a given time step, the Monte-Carlo transition of an agent from one state to another, or from one position to an adjoining grid space, is governed by a probability that depends on the cell environment, its history, and certain adjustable parameters. The value of a random number ("coin toss") determines whether the transition occurs or not. Cell motion can have directed (e.g. chemotactic) as well as random component. In this respect, the simulation is a so-called "lattice-gas" type of Cellular Automata (CA). The motion of the cells takes place once per time

TABLE A3

Typical parameters associated with cytokines binding to the cell-surface receptors

Cytokine	k_f ($nM^{-1}min^{-1}$)	k_b(min^{-1})	$K_D = k_b/k_f$ (nM)	Receptors/cell	Reference
IL-6 (mouse)			2.25	300–720	[1]
IL-6	0.013	0.054	4.3		[2]
Human interleukin DA (high affinity)	2.4	0.0084	3.8×10^{-3}	20–600	[3]
Human interleukin DA (low affinity)	0.072	0.18	2.6	1000–5000	[3]
IL-1 human B-lymphoma			2.1	7709	[4]
IL-1 murine thymoma cell			0.15		[5]
IL-1 beta			1.0		[6]
TNF mouse leukemia			Human TNF 1.7–2.8	4–5000	[7]
TNF alpha Overexpressing Human cells			0.2	94 000	[8]
TNF alpha recombinant human			1.3	1100	[9]

Note: Data from [1] Yamaguchi *et al.* (1992), [2] Hammacher *et al.* (1996), [3] Godard *et al.* 1992, [4] Horuk et al. (1987), [5] Dripps *et al.* (1991), [6] Benjamin *et al.* (1990), [7] Michishita *et al.* (1990) [8] Pennica et al. (1992), [9] Ding *et al.* (1989). A cell of volume V (in μm), with r receptors on its surface, results in a local "effective concentration" of receptors 1.655 (r/V) nM. Typical cell volumes are taken to be $V = 1000$–$1300\,\mu m^3$.

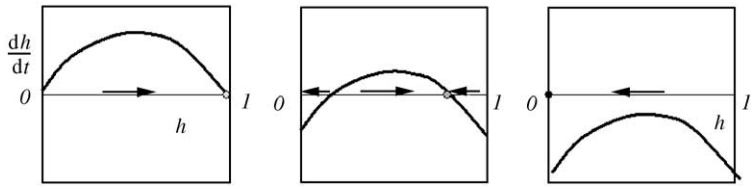

FIG. A1. Neuronal health is represented by an aggregate value which ranges from $h = 1$ (or 100%) for full health to $h = 0$ for dead neurons. Shown here is the rate of change of neuronal health (dh/dt) as a function of current health (h) for three values of the injurious influence, I. The directions of the arrows indicate increasing health (to the right) or decreasing health (to the left). (a) No injurious influence ($I = 0$): health increases up to full recovery at $h = 1$ regardless of the initial state. (b) $0 < I < r/4$: intermediate level of toxicity. Here neurons will become partially stressed (i.e. approach the steady state marked by heavy dot) unless they are already in very low health. In the latter case, they would die. (c) $I > r/4$: this is a fatal level of toxicity and all states lose health and die unless the toxic influence is removed.

step, DT. Grid spaces occupied by astrocytes, or too many microglia exclude new cells.

In the simulation, microglia stick to amyloid fibers. The probability of immobilization, P_I, in a given time step and the probability, P_S, of a cell to remain stuck to fiber in the presence of soluble amyloid is based on data in El Khoury *et al.* (1996). We have also assumed that these probabilities have the forms

$$P_I = \frac{F}{F+G}, P_s = \mathrm{e}^{-kS},$$

where G, k are adjustable parameters.

AMYLOID FIBER GROWTH AND NUCLEATION

The rules governing fibrous and soluble amyloid are given below. We define the following notation: S is the concentration of soluble amyloid and f is the fiber concentration at a given site, F_{max} is the maximal fiber level per site allowed in the simulation, F is a weighted average of local fiber concentration (ij fibers weighted double those in surrounding eight grid sites $i \pm 1$, $j \pm 1$), q is the concentration of microglia at the given site. Then changes in the levels of fibrous and soluble amyloid can be represented by a stochastic, discretized version of the set of equations below (with time step DT):

$$\frac{\mathrm{d}S}{\mathrm{d}t} = -R_1(S-b)F - R_1(S-b)^2 - k_2 q \frac{S}{h+S},$$

$$\frac{\mathrm{d}f}{\mathrm{d}t} = R_2(S-b)F + R_1(S-b)^2 + n\frac{F}{F_{\max}} - k_1 q f.$$

Growth and elongation of pre-existing fibers (first terms in both equations) occur only when the level of soluble amyloid exceeds some critical value, $S > b$, and the rate of conversion is then governed by the parameter R. If $S < b$, this term is omitted. *De novo fiber nucleation* (second term in equations) similarly occurs given a sufficiently high level of soluble amyloid, $S > b$, and results in new "seeds" or nuclei for fiber deposits. The quadratic dependence on amyloid concentration represents the fact that this step is rate-limiting. If $S < b$, this term is omitted. *New fibers adjoining a deposit*: an empty site adjoining a site containing fibers can be nucleated *de novo* with probability that depends on a parameter n. *Soluble amyloid removal* by microglia (last terms in both equations) follows Michaelis–Menten kinetics for the soluble form with parameters k governing the maximum uptake rate, and h the amyloid concentration at which the binding is half-maximal. Microglia cannot absorb amyloid in excess of some maximal capacity. *Fibrous amyloid removal* by microglia occurs by a distinct mechanism of phagocytosis at an assumed 10% of the uptake rate for the soluble form. There is currently no limit on the amount of fiber that can be ingested by a cell.

Neurons that have been exposed to IL-1B in excess of the level that triggers a new source are tested once by random draw to determine if they can give rise to new sources of amyloid-beta under the appropriate conditions. An amyloid source at the site of a dead neuron is removed.

RATES OF SECRETION

Microglia that have taken up amyloid in excess of some threshold level secrete the cytokine IL-1B. Similarly, astrocytes secrete IL6 and TNF-α once they have absorbed sufficient IL-1B. The rates of secretion have been calculated from data in the literature (Table A2). We assume that the amount secreted per unit time per cell is constant so long as the stimulus to secrete is in effect. Chemical secretion is calculated on the micro time step dt.

CYTOKINE RECEPTOR KINETICS

We use a Michaelis–Menten formulation for cytokine-receptor binding kinetics and cytokine uptake by cells: for C the cytokine concentration, we discretize the equation

$$\frac{\mathrm{d}C}{\mathrm{d}t} = -K_{\max}\frac{C}{k_n + C},$$

where $K_{\max}$ is a maximal uptake rate, and k_{n} the half-maximal chemical concentration. Standard assumptions of Michaelis–Menten kinetics (e.g. see Edelstein-Keshet, 1988) lead to $K_{max} = k_2\ R$ and $k_n = (k_b{+}k_2)/k_f$, where R is the total (local) concentration of receptors, k_f , k_b are forward and reverse-binding constants for ligand to cell-surface receptor, and k_2 is the rate of processing of receptor–ligand complex. Typical values of the cytokine receptor equilibrium constants $K_D = k_b/k_f$ are shown in Table A3. The value of k_2 was estimated as $1.0\,\mathrm{s}^{-1}$. This is taken to reflect a typical time-scale pertaining to early signal transduction events mediated by membrane-bound receptors.

ASTROCYTE MOTION AND STATES

In the simulation, the state of each astrocyte toggles between *inactive* and *receptive* as the IL-1B concentration nearby rises above or falls below a triggering level. Beyond a second IL-1B concentration threshold, the cell has a probability of becoming *motile*. With some probability, a *receptive* or *motile* astrocyte will move a short distance towards nearby amyloid fiber (with superimposed random motion), but not into a site currently occupied by microglia, fiber, or too many other astrocytes. The maximum speed of an astrocyte is $0.1\,\mu\mathrm{m\ min}^{-1}$ (Kornyei *et al*., 2000). When the astrocyte senses amyloid fiber in any of the eight adjoining grid sites, the cell changes to a *blocking* state with some probability. This leads to reduction in the diffusion coefficients at the site: the value D_{ij} is scaled by $(1\text{-}w)^m$ where w is an adjustable parameter and m is the number of blocking astrocytes at the affected grid sites.

NEURONS

Neuronal health has a value $0 < h < 1$ at each grid site, with initially full health, $h(0) = 1$ everywhere, and subsequently $\mathrm{d}h/\mathrm{d}t = rh(1-h)–I$, at each site, so long as $h > H_{min}$, where H_{min} is a critical health level below which there is no recovery. If $h < H_{min}$, the rule is $\mathrm{d}h/\mathrm{d}t = -I$.

Possible outcomes of neuron health dynamics at a given site are shown in Fig. A1. (i) If there is no local toxicity ($I = 0$), full recovery occurs. (The stable steady state, $h = 1$ is an attractor for all $H_{min} < h < 1$.) (ii) Where toxicity is high, ($I > r/4$), neurons die. (All states in $0 < h < 1$ are attracted to $h = 0$.) (iii) Where toxicity is sub-lethal ($\mathrm{I} < \mathrm{r}/4$), the outcome depends on the current state: neurons in poor health will die, neurons in good health will recover partially. (The upper steady state is depressed, signifying lowered steady-state health, and the range of health associated with mortality increases.)

The overall neuron health shown in Fig. 5 is the average health over all $n = 40 \times 40$ sites, $\boldsymbol{H} = (1/n)\ \Sigma h_I$, where h_i is the health of the i-th neuron site.

COMMENTS ABOUT NUMERICAL METHODS

In simulating chemical diffusion, several distinct methods (Strikwerda,1989; Press *et al*., 1988) were implemented and tested rigorously against one another, and against simple settings in which analytic calculation of diffusion methods could be used for comparison (e.g. diffusion from a point source in a homogeneous domain).We briefly describe our experiences with several of these methods here:

- Simple explicit scheme (Strikwerda, 1989). Problem encountered: failure of material conservation.

- Implicit scheme with LU decomposition of an $n^2 \times n^2$ matrix (Press *et al.*, 1988). Problem encountered: Matrix multiplication is expensive and computing matrix inverse is memory intensive. As soon as diffusivities change (due to astrocytes), the inverse must be recomputed at great expense. (Note: matrix is not tri-diagonal because computing diffusion in more than one dimension leads to more non-zero off-diagonal bands.)
- Alternating Direction Implicit (ADI) with Peaceman–Rachford Algorithm (Press *et al.*, 1988). Problem encountered: accuracy requires a step size of 1/40 min which results in same speed as the explicit method with a step size of 1/80 min.
- Explicit scheme based on flux balance. Computed the flux to follow diffusion for non-uniform diffusivities. Limitations: Step-size is restricted due to stability of the scheme, but this was found to be the best method in terms of ease of use and memory usage for our purposes.